

The role of semi-volatile organic compounds in the mesoscale evolution of biomass burning aerosol: a modeling case study of the 2010 mega-fire event in Russia

I. B. Konovalov¹, M. Beekmann², E. V. Berezin¹, H. Petetin², T. Mielonen³, I. N. Kuznetsova⁴, and M. O. Andreae⁵

¹Institute of Applied Physics, Russian Academy of Sciences, Nizhny Novgorod, Russia

²Laboratoire Inter-Universitaire de Systèmes Atmosphériques, CNRS, Université Paris-Est and Université Paris 7, Crèteil, France

³Finnish Meteorological Institute, Kuopio, Finland

⁴Hydrometeorological Centre of Russia, Moscow, Russia

⁵Biogeochemistry Department, Max Planck Institute for Chemistry, Mainz, Germany

Correspondence to: I. B. Konovalov (konov@appl.sci-nnov.ru)

Abstract. Chemistry transport models (CTMs) are an indispensable tool for studying and predicting atmospheric and climate effects associated with carbonaceous aerosol from open biomass burning (BB); this type of aerosol is known to contribute significantly to both global radiative forcing and to episodes of air pollution in regions affected by wildfires. Improving model performance requires systematic comparison of simulation results with measurements of BB aerosol and elucidating possible reasons for discrepancies between them, which, by default, are frequently attributed in the literature to uncertainties in emission data. Based on published laboratory data on the atmospheric evolution of BB aerosol and using the volatility basis set (VBS) framework for organic aerosol modeling, we examined the importance of taking gas-particle partitioning and oxidation of semi-volatile organic compounds (SVOCs) into account in simulations of the mesoscale evolution of smoke plumes from intense wildfires that occurred in western Russia in 2010. Biomass burning emissions of primary aerosol components were constrained with PM₁₀ and CO data from the air pollution monitoring network in the Moscow region. The results of the simulations performed with the CHIMERE CTM were evaluated by considering, in particular, the ratio of smoke-related enhancements in PM₁₀ and CO concentrations (Δ PM₁₀ and Δ CO) measured in Finland (in the city of Kuopio), nearly 1000 km downstream of the fire emission sources. It is found that while the simulations based on a “conventional” approach to BB aerosol modeling (disregarding oxidation of SVOCs

and assuming organic aerosol material to be non-volatile) strongly underestimated values of Δ PM₁₀/ Δ CO observed in Kuopio (by a factor of two), employing the “advanced” representation of atmospheric processing of organic aerosol material resulted in bringing the simulations to a much closer agreement with the ground measurements. Furthermore, taking gas-particle partitioning and oxidation of SVOCs into account is found to result in a major improvement of the agreement of simulations and satellite measurements of aerosol optical depth, as well as in considerable changes in predicted aerosol composition and top-down BB aerosol emission estimates derived from AOD measurements.

1 Introduction

Carbonaceous aerosol originating from open biomass burning (BB) plays a major role in the atmosphere by affecting both climate processes and air quality (Andreae and Merlet, 2001; Langmann et al., 2009). In particular, BB is estimated to provide about 40 % of the atmospheric budget of black carbon (BC) (Bond et al., 2013), which contributes significantly to climate forcing (IPCC, 2013; Andreae and Ramanathan, 2013). BB emissions are also known to be a major source of particulate organic matter (POM), which contributes to both direct and indirect radiative forcing by providing absorbing brown carbon (e.g., Chakrabarty et al., 2010; Saleh et al., 2014), enhancing light absorption by BC (up to a fac-

tor of two) due to the lensing effect (Jacobson, 2001), as well as contributing to the light scattering (Keil and Haywood, 2003). Episodes of a major impact of aerosol emissions from fires on regional air quality have been reported worldwide (e.g., Heil and Goldammer, 2001; Andreae et al., 2002; Sinha et al., 2003; Bertschi and Jaffe, 2005; Konovalov et al., 2011; Strand et al., 2012; Andreae et al., 2012; Engling et al., 2014). Therefore, the physical and chemical properties of BB aerosol, and its sources and evolution have to be adequately represented in atmospheric numerical models aimed at analyzing and predicting climate change and air pollution phenomena (e.g., Kiehl et al., 2007; Goodrick et al., 2012).

Meanwhile, there are indications that the available chemistry transport models (CTMs) simulating sources and atmospheric evolution of BB aerosol are not always sufficiently accurate. For example, the concentrations of aerosol originating from wildfires in Central America were systematically underestimated (by about 70 %) in simulations performed by Wang et al. (2006) with the RAMS-AROMA regional transport model (in spite of the fact that the variability of the aerosol concentration was well captured in the simulations). Predictions of surface aerosol concentrations in California from the BlueSky Gateway (Strand et al., 2012) air quality modeling system were found to be in acceptable range of the observed values in one part of the model domain (specifically, in northern California), but negatively biased in the other part of the domain (southern California). Large regional biases in AOD simulations performed with the global GOCART CTM were found by Petrenko et al. (2012). Kaiser et al. (2012) found that in order to achieve a reasonable agreement of global simulations of aerosol optical depth (AOD) with corresponding satellite measurements, the BB aerosol emissions specified in the ECMWF integrated forecast system had to be increased globally by a factor of 3.4. Using AOD and carbon monoxide (CO) satellite measurements analyzed in combination with outputs of the mesoscale CHIMERE CTM, Konovalov et al. (2014) found (qualitatively similar to the results of Kaiser et al., 2012) that the ratios of aerosol and CO emissions from forest and grassland fires in Siberia are likely to be about a factor of 2.2 and 2.8 larger than those calculated with typical emission factors from literature. In contrast, Konovalov et al. (2011) showed that in order to fit the CHIMERE simulations to ground based observations during wildfires in western Russia, the BB aerosol emissions had to be scaled with a factor of about 0.5 relative to the CO emissions.

Although most modeling studies tend to attribute systematic discrepancies between simulations and atmospheric observations of BB aerosol to uncertainties in the fire emission inventories, it seems also quite probable that at least a part of the discrepancies may be due to deficiencies in the modeling representation of BB aerosol processes. Indeed, for the special case of organic aerosol (OA) originating from fossil fuel burning, it has been argued (e.g., Shrivastava et al., 2006; Donahue et al., 2006; Robinson et al., 2007) that ad-

equated models of OA evolution require taking into account the volatility of primary OA (POA) compounds as well as the formation of secondary OA (SOA) from oxidation of semi-volatile organic compounds (SVOC) in the atmosphere. Furthermore, laboratory measurements indicated that, like the POA emissions from fossil fuel burning, BB aerosol emissions feature a broad spectrum of volatility (e.g., Lipsky and Robinson, 2006; Grieshop et al., 2009a; Huffman et al., 2009; May et al., 2013) and may be subject to rapid oxidation processes leading to formation of substantial amounts of SOA (Grieshop et al., 2009b; Hennigan et al., 2011, 2012; Heringa et al., 2011; Donahue et al., 2012; Ortega et al., 2013). An increase of BB aerosol mass or particle number concentration was also diagnosed in some field studies (Hobbs et al., 2003; Yokelson et al., 2009; Akagi et al., 2012). Recently, Vakkari et al. (2014) showed evidence for substantial growth and increasing oxidation state of biomass burning aerosols during the first few hours of atmospheric transport. Meanwhile, all the chemistry transport models employed in the above-mentioned simulations of BB aerosol evolution treated the primary aerosol emissions as non-volatile, and only the oxidation of several definite volatile organic compounds (VOCs) was taken into account as a source of SOA in some of the models.

A convenient framework enabling robust and computationally efficient representation of the thermodynamics and chemistry of organic gases and particles in CTMs, known as the volatility basis set (VBS) framework was introduced by Donahue et al. (2006). Several studies employed this framework for modeling the evolution of OA from anthropogenic (fossil fuel burning) and (in some cases) biogenic emissions and found that it provides reasonable agreement between simulations and measurements (see, e.g. Lane et al., 2008; Murphy and Pandis, 2009; Farina et al., 2010; Hodzic et al., 2010; Tsimpidi et al., 2010; Shrivastava et al., 2011; Ahmadov et al., 2012; Zhang et al., 2013). Hodzic et al. (2010), Bergström et al. (2012) and Shrivastava et al. (2015) used the VBS method to model atmospheric processing of BB aerosol along with OA from other sources, but did not attempt to isolate effects of potentially large uncertainties in BB emissions from those associated with the modified representation of OA processes.

The main goal of this study is to examine the impact of using the advanced approach to modeling of OA processes instead of the conventional one on the simulated evolution of BB aerosol in an important (though episodic) situation when BB was a major source of OA. We parameterize the BB aerosol processes by using data from dedicated laboratory measurements and apply our model to the case of the mega-fire event that occurred in Western Russia in summer 2010 as a result of an abnormal heat wave (Barriopedro et al., 2011). This event provided abundant observational material for the critical evaluation of our current understanding of atmospheric effects of wildfires and has already received considerable attention in the scientific literature (Elansky et al.,

2011; Konovalov et al., 2011; Mei et al., 2011; Witte et al.,
2011; Golitsyn et al., 2012; Huijnen et al., 2012; Krol et al.,
2013; Popovicheva et al., 2014). However, to the best of our
knowledge, there has been no study yet focusing on modeling
the evolution (“ageing”) of aerosol in BB plumes from
these fires. By considering this special case, we intend to ex-
amine the feasibility and benefits of using the VBS approach
for modeling aerosol evolution in BB plumes, especially at
temporal scales considerably exceeding those addressed in
typical laboratory measurements. In general, this study is in-
tended to contribute to advancing current understanding of
BB aerosol processes and their representation in chemistry
transport models.

This paper is organized as follows: Section 2 describes
our modeling framework; in particular, it outlines the meth-
ods and parameterizations representing BB aerosol emis-
sions and evolution and defines the scenarios of our numeri-
cal experiments. The results of the numerical simulations are
presented in comparison with data from in-situ and satellite
measurements in Section 3, which also discusses the implica-
tions of the results of our simulations for predicting aerosol
composition and estimation of emissions from wildfires by
using the “top-down” approach. Our findings are discussed
in the context of earlier studies of BB aerosol in Section 4.
A summary of the results of this study and some concluding
remarks are provided in Section 5.

2 Model and measurement data description

2.1 The CHIMERE CTM: general characteristics

This study is based on using the CHIMERE CTM, which
is a typical Eulerian off-line model designed for simulating
and predicting air pollution at the regional and continental
scales. It includes parameterizations of most important phys-
ical and chemical processes affecting the atmospheric evolu-
tion of aerosols of various types and origins (such as primary
anthropogenic, dust, biogenic, sea spray, secondary inorganic
and organic aerosols) and gaseous air pollutants. These pro-
cesses include, in particular, emissions of gases and aerosols
(the anthropogenic and biogenic emission interfaces enable
calculation of the emissions on a model grid from data of
corresponding emission inventories), chemical transforma-
tion of tens of compounds due to gas-phase and heteroge-
neous reactions, absorption/desorption of some semi-volatile
species by/from aerosol particles, advection and turbulent
mixing of gases and aerosols, and their dry and wet deposi-
tion. The detailed description of CHIMERE and examples of
its numerous applications are provided in Menut et al. (2013)
and in the CHIMERE documentation available online along
with the model codes at <http://www.lmd.polytechnique.fr/chimere>.

While most earlier CHIMERE applications addressed con-
tributions to atmospheric composition from anthropogenic

and biogenic sources, it was also successfully applied in sev-
eral studies focusing on the atmospheric effects of fire emis-
sions (Hodzic et al., 2007; Konovalov et al., 2011, 2012,
2014; Péré et al., 2014). In particular, simulations performed
with CHIMERE were found by Konovalov et al. (2011) to
be in good agreement with air quality monitoring data in
Moscow during the extreme air pollution event caused by
wildfires in 2010. The same event and similar data are con-
sidered in this study. The CHIMERE configuration is similar
to that in the studies by Konovalov et al. (2011, 2014), except
for some changes and updates mainly applied to our method
aimed at deriving fire emissions from satellite measurements
of fire radiative power (FRP) (Ichoku and Kaufman, 2005).

2.2 Basic model configuration

Gas-phase processes were simulated with the reduced chem-
ical mechanism MELCHIOR2 (Derognat et al., 2003; Menut
et al., 2013) including about 120 reactions of 40 species.
Menut et al. (2013) found that the performance of this com-
putationally efficient mechanism in the case of ozone simu-
lations was very similar to that of a much more com-
plex mechanism, such as SAPRC07 (Carter, 2010). Photol-
ysis rates were calculated with the TUV model (Madronich
et al., 1998) embedded in CHIMERE as a function of AOD
derived from Moderate-resolution Imaging Spectroradiome-
ter (MODIS) measurements (see Konovalov et al., 2011,
for further detail). Evolution of secondary inorganic aerosol
was simulated with the tabulated version of the thermo-
dynamic model ISORROPIA (Nenes et al., 1998). Anthro-
pogenic emissions of gases and aerosol were specified by
using the EMEP (European Monitoring and Evaluation Pro-
gramme) inventory data (EMEP/CEIP, 2014) for the year
2010. Anthropogenic primary aerosol emissions were dis-
tributed among nine size bins with diameters from 20 nm
to 10 μm by assuming a bimodal log-normal size distribu-
tion with a mass mean and standard deviation of 0.11 μm
and 1.6 for the fine mode and of 4 μm and 1.1 for the course
mode, respectively (accordingly to the CHIMERE standard
settings). Biogenic emissions (including those of aerosol pre-
cursors) were calculated by using the standard CHIMERE
interface and data from the MEGAN (Model of Emissions
of Gases and Aerosols from Nature) model (Guenther et al.,
2006) for emissions from vegetation, and the European in-
ventory of soil NO emissions by Stohl et al. (1996). Dust
aerosol emissions were taken into account by using a sim-
ple parameterization developed by Vautard et al. (2005). The
monthly climatological data from the LMDz-INCA global
model (Folberth et al., 2006) were used as initial and bound-
ary conditions for our simulations.

Apart from using the standard model output data for con-
centrations of gaseous and aerosol species, we considered
AOD at 550 nm; it was evaluated in the same way as in Kono-
valov et al. (2014) following a robust method, proposed by
Ichoku and Kaufman (2005). Specifically, AOD was derived

from simulated aerosol mass column concentrations by applying the mass extinction efficiency. We took into account that a predominant part of atmospheric aerosol loading in the situation considered was due to biomass burning and chose this coefficient to be the same as in Konovalov et al. (2014) ($4.7 \pm 0.8 \text{ m}^2 \text{ g}^{-1}$), based on the experimental data by Reid et al. (2005b). Some bias in AOD values calculated in this way may be associated with relatively small (in the case considered) contributions of anthropogenic, biogenic, and dust aerosols, whose mass extinction efficiency is different from that of BB aerosol. We evaluated this bias as the mean relative difference between the simulated and measured AOD in the grid cells on the days where and when the contribution of BB aerosol was negligible (see Konovalov et al., 2014, for further detail); the bias was then subtracted from the simulated AOD values.

The evolution of BB plumes was simulated with a resolution of 0.5 by 0.5° and twelve layers in the vertical; the upper layer corresponded to the 200 hPa pressure level. The study region (corresponding to the model domain) covers most of European Russia (including the Moscow region) and a part of Eastern Europe ($48\text{--}66^\circ \text{ N}$; $20\text{--}56^\circ \text{ E}$). The simulations were performed for the period from 12 July to 20 August 2010. The first three days were reserved for the model's "spin-up"; therefore, the period of our analysis begins on 15 July.

The WRF-ARW (v.3.6) model (Skamarock et al., 2005) was used as a meteorological driver for CHIMERE. The meteorological data were calculated on a $50 \text{ km} \times 50 \text{ km}$ grid with 30 levels extending in the vertical up to the 50 hPa pressure level. The Mellor–Yamada–Janjic (Eta) scheme (Janjic, 1994) was used for the simulation of boundary layer processes together with the Eta similarity scheme (based on the Monin–Obukhov theory) for surface physics (Janjic, 1990). Note that the meteorological situation in the region and period considered featured unusually hot temperatures (in particular, daily maximum temperature in Moscow was in the range from 29° C to 38° C), almost absent precipitation, and a blocking anticyclonic circulation that started to form at the end of July and was persistent until the second half of August (see, e.g., Konovalov et al., 2011; Witte et al., 2011).

In this study, we considered two different approaches to modeling BB OA evolution. The first approach, which is implemented in the standard version of CHIMERE, assumes that OA particles consist of non-volatile material. The second approach is based on the absorptive partitioning theory and has been implemented in our version of CHIMERE by using the volatility basis set (VBS) framework (Donahue et al., 2006; Robinson et al., 2007; Lane et al., 2008); note that the VBS framework was already used in dedicated versions of the CHIMERE model for simulating OA originating mostly from fossil fuel burning (Hodzic et al., 2010; Zhang et al., 2013). Implementation of these two approaches in the CHIMERE version used in this study is described below in Sections 2.3 and 2.4, respectively.

2.3 Representation of BB OA processes in the “standard” version of CHIMERE

Aerosol particles emitted from fires are conventionally assumed to consist of non-volatile POM and BC. Therefore, they cannot evaporate and can be lost only as a result of deposition and transport outside of the model domain. A fine fraction of primary BB aerosol emissions is distributed according to a lognormal size distribution with a mass mean diameter of $0.25 \mu\text{m}$ and a standard deviation of 1.6 by taking into account a range of fresh smoke observations in temperate forest reported in the literature (see, e.g., Fiebig et al., 2003; Reid et al., 2005a, and references therein) and following Hodzic et al. (2007) and Konovalov et al. (2011). A coarse fraction of primary aerosol particles having a typical mean diameter of about $5 \mu\text{m}$ and usually contributing 10–30 % to the total mass of fresh aerosol emissions (and, probably, even a smaller part of organic carbon as indicated, e.g., by Alves et al., 2011) was disregarded to facilitate the comparative analysis of simulations performed with the standard and VBS method.

The formation of SOA is represented by absorption of semi-volatile compounds produced as a result of the oxidation of primary VOCs (Bessagnet et al., 2009; Hodzic et al., 2009); such compounds are referred below to as V-SOA. The yield of V-SOA from oxidation of VOCs from both fossil fuel and biomass burning is described by a single-step oxidation mechanism (Pun et al., 2006) as reactions of three lumped model VOC species (V-SOA precursors) with OH, O_3 and NO_3 producing several surrogate V-SOA species. These three lumped species are assumed to represent three classes of VOCs, such as a class of alkanes from C4 to C13, a class of mono-substituted aromatics including benzene, and a class of polysubstituted aromatics. The same single-step oxidation mechanism by Pun et al. (2006), with some modifications introduced following the formulations by Kroll et al. (2006) and Zhang et al. (2007), is used to represent the formation of V-SOA as a result of the oxidation of biogenic VOCs (for isoprene and terpenes). Further details regarding the representation of OA processes in the standard version of CHIMERE can be found elsewhere (Bessagnet et al., 2009; Hodzic et al., 2009; Menut et al., 2013).

2.4 Representation of BB OA processes in CHIMERE: the VBS framework

2.4.1 Representation of primary organic aerosol (POA) emissions from fires

Here, POA emissions (including all organic material that is assumed to have a potential to form OA particles under atmospheric conditions) are considered as semi-volatile and distributed into several volatility classes characterized by the reference saturation concentration C_i^* at 298 K, enthalpy of vaporization, ΔH_i , and the fraction in the total POA

emissions, f_i (where i is the index of a volatility class). The emission factors for total emissions of POA in both the gas and particle phases, β^{poa} , and for organic carbon in the particle phase (OC), β^{oc} , are assumed to be related as predicted by the absorptive partitioning theory (Pankow, 1994; Shrivastava et al., 2006):

$$\beta^{\text{poa}} = \beta^{\text{oc}} \eta \left[\sum_i f_i \left(1 + \frac{C_i^* \exp\left(-\frac{\Delta H_i}{R} \left(\frac{1}{T} - \frac{1}{298}\right) \frac{298}{T}\right)}{C_{\text{OA}}}\right)^{-1} \right]^{-1}, \quad (1)$$

where C_{OA} and T are the ambient OA mass concentration and temperature, R is the gas constant, and the factor η (assumed to be equal 1.8 here) is applied to convert OC into POM. In Eq. (1), the larger the ambient concentration C_{OA} and the smaller the saturation concentration C_i^* , the larger is the fraction of POA emissions in the particle phase, and thus the closer the ratio β^{poa} over $\beta^{\text{oc}} \eta$ is to unity. In contrast, for small C_{OA} and large C_i^* , a large part of POA emissions occurs in the gas phase and is not accounted for in measurements of particulate phase emissions. While the factors β^{oc} , characterizing emissions of OC in the particle phase from biomass burning, have been frequently measured both in laboratory and field studies (see, e.g., Andreae and Merlet, 2001; Akagi et al., 2011, and references therein) and are widely used in emission inventories (see, e.g., van der Werf et al., 2010), their values reported in the literature are usually not accompanied by corresponding data regarding C_{OA} and ambient temperature. Note that disregarding the gas-particle conversion processes may account for a part of the large discrepancies between different measurements of the emission factors. Therefore, there is a general problem of how to convert the measured values of β^{oc} into the values of β^{poa} , and some additional assumptions regarding the parameters of Eq. (1) were needed in order to overcome it in our case. Specifically, we assumed that $T = 298$ K and $C_{\text{OA}} = 10$ $\mu\text{g m}^{-3}$. For comparison, Vicente et al. (2013) reported that $\text{PM}_{2.5}$ concentrations during their emission factor measurements in the vicinity of wildfires in Portugal were in the broad range from 0.69 to 25 $\mu\text{g m}^{-3}$. In addition, we assumed that all POA were released into the atmosphere from fires as particles (as a result of the condensation process under very high ambient concentration of combustion products after their initial cooling). These assumptions do not have a significant effect on our simulations because the total BB aerosol emissions were constrained by measurements, as explained in Section 2.7. POA particulate emissions were distributed among nine size sections according to the same size distribution as described above for the standard method (see Section 2.3)

2.4.2 Volatility distributions

Volatility distributions of POA were specified by using the results of a dedicated laboratory study by May et al. (2013), in which a kinetic model was used to derive volatility distributions and enthalpies of vaporization from thermodynamic measurements of BB emissions. The POA emissions were distributed among seven volatility classes with C_i^* ranging from 10^{-2} to 10^4 . According to May et al. (2013), the derived volatility distributions are characterized by very large uncertainties (which likely reflect a part of the natural variability of volatility of smoke from burning of different types of biomass). For example, the fraction of organic material in the volatility class with $C_i^* = 10^4$ $\mu\text{g m}^{-3}$ was estimated to range from 0.3 to 0.7 if the accommodation coefficient equals unity (see Table S4 in May et al. (2013)). We tried to take into account this uncertainty by considering two different volatility distributions (see Table 1) corresponding to the accommodation coefficient equal unity.

Note that unlike most other studies employing the VBS framework, we do not consider so called intermediate volatile compounds (IVOCs) separately from semi-volatile compounds (SVOCs). Usually, a class of IVOCs is intended to represent organic compounds that are more volatile than SVOC but less volatile than VOCs, such that $10^4 \leq C_i^* \leq 10^6$ $\mu\text{g m}^{-3}$. Under typical environmental conditions, the contribution of IVOCs to the particle phase is assumed to be negligible, although they are still expected to provide a considerable source of SOA after their oxidation, at least in situations with predominant POA emissions from fossil fuel burning (see, e.g., Robinson et al., 2007). However, on the one hand, this study addresses a special situation with OA concentration reaching (in simulations) values of about 3000 $\mu\text{g m}^{-3}$: obviously, under such conditions, organic compounds with $C_i^* \sim 10^4$ $\mu\text{g m}^{-3}$ should be treated as semi-volatile. On the other hand, there is evidence that BB emits less IVOCs than motor vehicles (Grieshop et al., 2009a), and that they do not contribute significantly to SOA formation. Although the contribution of IVOCs to SOA was not necessarily negligible in the situation considered, their emissions were not included in our simulations, as May et al. (2013) did not provide any data regarding emissions of compounds with $C_i^* > 10^4$ $\mu\text{g m}^{-3}$.

To ensure numerical stability of our calculations, evaporation of POA in the two lowest volatility classes (with $C_i^* = 0.01$ $\mu\text{g m}^{-3}$ and $C_i^* = 0.1$ $\mu\text{g m}^{-3}$) was disabled. This restriction did not affect our results, since typical OA concentrations in the smoke plumes considered were much higher (> 10 $\mu\text{g m}^{-3}$) even after strong dilution.

2.4.3 Multi-generation oxidation of POA compounds

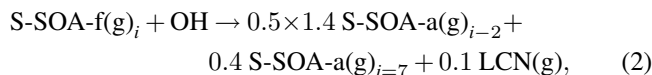
The POA species were assumed to be subject to gas-phase oxidation, which was represented by the reaction of the gas-phase fraction of POA (POA(g)) with OH. The oxidation

mechanism was parameterized by using two different methods described in this and the next sections. The first method represents the oxidation of POA(g) as a multi-stage process. It is based on the estimates derived by Grieshop et al. (2009b) from laboratory measurements of the oxidation of BB smoke from a wood stove; some modifications explained below are introduced following Shrivastava et al. (2013, 2015). Specifically, similar to Grieshop et al. (2009b) we assumed that each reaction of POA(g) with OH reduced the volatility of organic gases (from a given volatility class) by a factor of 100 (leading to a two-bin shift in the volatility distribution) and increased the organic compound mass by 40 %; the reaction rate constant was set to be $2 \times 10^{-11} \text{ cm}^{-3} \text{ molecules}^{-1} \text{ s}^{-1}$. Evolution of semi-volatile species (called below S-SOA) produced from oxygenation of POA was simulated in two different ways. In the first way, following Grieshop et al. (2009b) we represented oxidation of S-SOA as that of POA (that is, by assuming that S-SOA were governed by partitioning theory and experienced successive gas-phase oxidation (functionalization) at the same rate and mass increment as POA). However, there is strong evidence (e.g., Chacon-Madrid and Donahue, 2011; Kroll et al., 2011; Donahue et al., 2012) that a chain of successive functionalization reactions is usually terminated due to the fragmentation process, which reduces volatility and limits the O : C ratio of oxygenated organic compounds. Accordingly, in the second way, we tried to take into account not only functionalization but also fragmentation reactions.

To represent fragmentation reactions we followed a simple method suggested by Shrivastava et al. (2013) and evaluated in Shrivastava et al. (2013, 2015). Rather than simulating O : C ratio within the VBS framework explicitly (as was suggested, e.g., by Donahue et al., 2012), Shrivastava et al. (2013, 2015) distinguished between different generations of oxidation and assumed that two first generations undergo only functionalization reactions, while products of the third and higher generations (which were lumped together) were subject to both functionalization and fragmentation reactions. A major difference between the VBS schemes used in this study and that in Shrivastava et al. (2013, 2015) is associated with the fact that we assumed each functionalization reaction to result in a two-bin shift in the volatility distribution (as indicated above) instead of the one-bin shift assumed by Shrivastava et al. (2013, 2015); thus two generations in the scheme by Shrivastava et al. (2013, 2015) are, effectively, equivalent to one generation in our scheme.

Accordingly, our VBS scheme that takes into account the fragmentation process involved “aged” S-SOA (S-SOA-a) species (representing second and higher generations of oxidation) along with first-generation S-SOA (S-SOA-f) species. We assumed that a reaction of POA species from the volatility bin “*i*” with OH yielded S-SOA-f species into the bin “*i-2*” and increased mass by 40 %. The reaction of S-SOA-f (or S-SOA-a) with OH was modeled according to the

following equation:



where the first and second terms in the right-hand side denote functionalization and fragmentation, respectively, LCN denotes low-carbon-number species (with high volatility), which are also a result of fragmentation, but (unlike S-SOA-a(g)_{*i=7*}) do not participate in any further reactions that may lead to SOA formation; the fractions of the functionalization (0.5) and fragmentation (0.4 and 0.1) pathways were chosen, for definiteness, to be the same as in the “Frag1” scheme in Shrivastava et al. (2013). Note that a smaller fraction of the functionalization pathway (0.15) and a larger fraction of the main fragmentation pathway (0.75) were assumed by Shrivastava et al. (2013) in their “Frag2” scheme and in the schemes employed in Shrivastava et al. (2015); however, using the “Frag1” and “Frag2” schemes for modeling of SOA loadings over Mexico City resulted in a similar degree of agreement between the simulations and aircraft measurements (Shrivastava et al., 2013).

In our numerical experiments, we also tried to take into account available experimental evidence (Cappa and Wilson, 2011; Vaden et al., 2011; Shiraiwa et al., 2013) that the distribution of S-SOA compounds between gas-phase and particle phase can be affected by condensed-phase processes such as formation of heavy low-volatility macromolecules from smaller S-SOA species (that is, oligomerization) or transformation of quasi-liquid condensed organic matter to a glassy state. To represent such processes in our model, we again followed Shrivastava et al. (2013, 2015). Specifically, we assumed that condensed-phase S-SOA (including both S-SOA-f and S-SOA-a) forming SOA are transformed at a constant rate into non-volatile SOA (NVSOA) species which, once formed, do not affect partitioning of S-SOA between gas and condensed phases. The transformation time scale was set to be 5 hours (instead of 30 min in Shrivastava et al. (2015)) to minimize the inconsistency of our model with the formulations used in the analysis of laboratory measurements (conducted on time scales of several hours) in the studies by Grieshop et al. (2009b) and May et al. (2013), where the condensed-phase transformation was not explicitly taken into account. Note that the time scale assumed for condensed-phase transformation was still much smaller than the typical period of BB aerosol evolution considered in this study (tens of hours) and that reducing this time scale down to a half of an hour in a test simulation was not found to significantly affect modeling results.

Along with SOA formation resulting from the absorption of S-SOA, we took into account a minor (under conditions of this study) SOA source associated with multi-stage oxidation of “traditional” volatile SOA precursors. A modeling scheme accounting for this source was adapted from Zhang et al. (2013): it simulates the formation of V-SOA from ox-

idation of VOCs by using six lumped species representing SOA precursors and four volatility classes. The BB emissions of these lumped SOA precursors were aggregated from emissions of individual VOCs using the data of Andreae and Merlet (2001) with recent updates (in the same way as the emissions of other model organic species, see Sect. 2.6).

2.4.4 Single-generation mechanism of SOA formation from oxidation of POA species

As an alternative to the representation of POA gas-phase oxidation processes leading to SOA formation by means of a multi-stage mechanism, these processes were parameterized using a “surrogate species” representing a mixture of numerous organic compounds unspecified in available emission inventories, as proposed recently by Jathar et al. (2014). This parameterization, which had been obtained by fitting box model simulations to the data of the biomass burning laboratory experiments described in Hennigan et al. (2011), represents the gas-phase POA oxidation as a single-generation process and assumes that yields of S-SOA from the reactions of any POA(g) species with OH are similar to those from oxidation of n-pentadecane (C_{15} n-alkane). Accordingly, similar to Jathar et al. (2014) (see Table S3 and Eq. (1,2) in Supporting information therein) we assumed that the yields of S-SOA into the volatility bins with C_i^* equal 0.1, 1, 10 and $100 \mu\text{g m}^{-3}$ were 0.044, 0.071, 0.41, and 0.30, respectively; the S-SOA yields into the other volatility bins were assumed to be zero. Oxidation of S-SOA was ignored; note, however, that according to Jathar et al. (2014), the single-generation mechanism can account for some aging of S-SOA implicitly. In addition, consistent with the analysis in Jathar et al. (2014), we assumed that n-pentadecane represents not only POA species, but also a fraction (10 %) of the total non-methane VOC emissions from biomass burning.

Note that the experimental data by Hennigan et al. (2011) are likely more representative of a range of real biomass burning conditions (at least, in North America) than those obtained and analyzed by Grieshop et al. (2009b). Nonetheless, it was difficult to predict a priori which of the parameterizations would result in the best performance of our simulations in the special case analyzed in this study. Indeed, on the one hand, the range of conditions reproduced in our simulations significantly surpassed that addressed in the laboratory experiments. In particular, BB aerosol concentrations were, in many grid cells and time intervals, much higher (about $1000 \mu\text{g m}^{-3}$ and more) and duration of the aerosol evolution was much longer in the simulations (more than one day) than in the laboratory experiments (about $100 \mu\text{g m}^{-3}$ and less, and several hours, respectively). Besides, ageing of aerosol emissions from many kinds of fuels typical for European Russia (e.g. Scotch pine, Norway spruce, elm, birch, etc.) has not yet been investigated in the laboratory. On the other hand, even the existing laboratory studies (Jathar et al., 2014; Grieshop et al., 2009b) indicated a large variability of

the SOA yields in separate experiments, which was not reproduced by box models employing the parameterizations outlined above. Note also that a potentially important limitation of the single-generation mechanism described above is associated with the fact that the SOA mass yields were fitted to the results of smog chamber experiments that typically span only several hours: accordingly, it can, in principle, be expected to underestimate SOA formation in situations (as one considered in this study) when aerosol daytime evolution takes several tens of hours.

2.5 Spatial and temporal allocation and speciation of fire emissions

Below, we outline our calculations of fire emissions by paying special attention to changes with respect to the previous studies, where a similar method was used. Fire emissions for a species s at time t , $E^s(t)$ ($\text{g s}^{-1} \text{m}^{-2}$), were calculated as follows:

$$E^s(t) = \Phi_d \sum_l \alpha_l \beta_l^s \rho_l h_{el}(t) C(\tau), \quad (3)$$

where Φ_d (W m^{-2}) is the daily mean FRP density derived from daily maxima of FRP in a given cell of the model grid, α_l ($\text{g}[\text{dry biomass}] \text{s}^{-1} \text{W}^{-1}$) is the factor converting FRP to the biomass burning rate (BBR) (below, we refer to this factor as the FRP-to-BBR conversion factor) for a given land cover type l , β_l^s ($\text{g}[\text{model species}] \text{g}^{-1}[\text{dry biomass}]$) are the emission factors, ρ_l is the fraction of the land cover type l , h_{el} is the assumed diurnal variation of fire emissions, and C is an additional ad hoc correction factor specified as a function of AOD at 550 nm wavelength, τ . This relationship follows a popular approach to calculation of fire emissions, which was proposed by Ichoku and Kaufman (2005) and has been used in a number of studies (see, e.g., Sofiev et al., 2009; Kaiser et al., 2012; Kononov et al., 2014, and references therein) since then. The factor C , which was initially introduced in Kononov et al. (2011), is intended to compensate for a possible attenuation of FRP measured from satellites by very heavy smoke from intense fires in the region and period considered; it is also assumed to account for the part of emissions from peat fires invisible from space but coinciding with visible forest or grass fires.

For convenience, we express the factor α as the product of its “a priori” value, α_0 , and the “a posteriori” correction factor, F_α :

$$\alpha = \alpha_0 F_\alpha. \quad (4)$$

Taking into account the experimental data by Wooster et al. (2005), α_0 is taken to be $3.68 \times 10^{-4} \text{g}[\text{dry biomass}] \text{s}^{-1} \text{W}^{-1}$, and different estimates of F_α are inferred from atmospheric measurements as explained in Section 2.7.

Similar to Kononov et al. (2011, 2014), the daily mean FRP density is evaluated by selecting daily maxima of the

FRP density in each model grid cell and by scaling them with the assumed diurnal cycle of the FRP maxima, h_{ml} :

$$\Phi_d = \frac{\max\{\Phi_k, k = 1, \dots, K\}}{\sum_l \rho_l h_{ml}(t_{\max})} \quad (5)$$

where k is the satellite orbit index, h_{ml} is the assumed diurnal distribution of the FRP daily maxima, and t_{\max} is the moment of time when the daily maximum of FRP is observed. The initial calculations of fire emissions were made on a grid of a higher resolution (0.25 by 0.1 °) to minimize the effect of cloud and smoke contamination on the selected FRP daily maximum values; these emission data were then projected onto the model grid. The temporal resolution of the emission data was 1 h.

While Eq. (3) in combination with Eq. (4), is very similar to Eq. (5) in Konovalov et al. (2011), there are a few noteworthy differences between them. First, in this study, we do not consider the peat fires explicitly. Although the attempt to estimate the emissions from peat fires (not visible from space), as described in Konovalov et al. (2011), was rather successful, this estimation was associated with a large uncertainty, which would only hinder evaluation of different modeling scenarios in this study. Note, however, that we still take peat fires into account implicitly by adjusting the FRP-to-BBR conversion factor. For similar reasons, we assume that the same FRP-to-BBR conversion factor value (and the same value of the correction factor, F_α) is applicable to both forest and grass fires (visible from space).

Second, for convenience, we normalize the factor $C(\tau)$ such that its average over the whole study region is equal to unity. Note that, following Konovalov et al. (2011), we define $C(\tau)$ to be proportional to $\exp(\tau)$; introducing this factor was found to drastically improve the agreement of our simulations with air pollution measurements in Moscow.

Third, instead of assuming very strong diurnal variation of fire emissions (see Konovalov et al., 2011, and Fig. 1 therein), we derived the diurnal cycle of the emissions directly from FRP observations using the method and formulations proposed by Konovalov et al. (2014) (see Eqs. 5 and 6 therein). In this study, we attempted to advance this method further by distinguishing between the diurnal cycle of FRP, h_{ml} , and that of emissions, h_{el} . To estimate the latter, the formulations given in Konovalov et al. (2014) were applied to all available FRP data, while the former was derived only from FRP daily maxima (exactly in the same way as in Konovalov et al. (2014), where h_{el} was implicitly assumed to be equal to h_{ml}). The diurnal cycles specified in this study for agricultural and grass fires, and (separately) for forest fires are shown in Fig. 1. Finally, the emission factors for organic carbon (OC), BC, CO, NO_x , and non-methane hydrocarbons (NMHC) (see Table 2) were specified using their average (over available measurements in extratropical forest) values from an updated dataset (M.O. Andreae, unpublished data, 2014) originally described in Andreae and Merlet (2001); emissions of individual VOCs were calculated by distribut-

ing the total NMHC emissions among the compounds represented in this database (proportionally to the average measured emission factors of these compounds) and then aggregating them into eleven lumped model species (similarly as it is done in the CHIMERE emission interface for anthropogenic emissions, see Menut et al., 2013). Note that the average emission factor values do not capture variability of fuel and combustion conditions in the region and period considered, but any more specific data were not available. POM emissions were obtained by scaling the OC emissions with a factor of 1.8, taking into account the typical range of OC/POM ratios observed in fire plumes and assumed in fire emission inventories (e.g., Alves et al., 2011; van der Werf et al., 2010).

Similar to Konovalov et al. (2014), the injection of fire emissions into the atmosphere was simulated by using the parameterization proposed by Sofiev et al. (2012). This parameterization enables evaluation of maximum plume height as a function of the FRP measured in a given fire pixel and of the Brunt–Väisälä frequency in the free troposphere. We consider this method as advantageous over a simpler method (assuming uniform distribution of fire emissions up to the height of one kilometer), which was employed in Konovalov et al. (2011), although no significant differences between results obtained with these two methods were revealed in the case of Siberian fires (Konovalov et al., 2014). We would like to emphasize that the changes in our calculations of fire emissions with respect to the previous studies affected the model performance only slightly and could not influence the major conclusions of this study.

2.6 Measurement data

Similar to Konovalov et al. (2011), we used the CO and PM_{10} measurements at the automatic air pollution monitoring stations of the State Environmental Institution “Mosecomonitoring” for calibration of fire emissions. We selected only those sites that provided both CO and PM_{10} data for at least 50 % of days during the period addressed in this study (from 15 July to 20 August 2010). These criteria were satisfied for four sites, including those located inside of the city of Moscow (“Kozhuhovo”, “MGU”) and in Moscow’s suburbs (“Pavlovskii posad” and “Zelenograd”). The selected stations were equipped with Thermo TEOM1400a and OPTEK K-100 commercial devices based on the Tapered Element Oscillating Microbalance and electrochemical methods employed for PM_{10} and CO measurements, respectively. The measurements were nominally taken three times per hour.

Along with the air pollution data from the Moscow region, we used simultaneous CO and PM_{10} measurements from the city of Kuopio, Finland (Portin et al., 2012). A Thermo TEOM 1400a and Monitor Labs 9830 B IR absorption CO analyzer were used for PM_{10} and CO measurements, respectively. By comparing relative perturbations of PM_{10} and CO in the Moscow region (that is, near the fires) and in Kuo-

pio (situated about 1000 km from Moscow), we attempt to elucidate the changes in BB aerosol mass due to transformation and loss processes in the atmosphere. The CO and PM₁₀ measurements in Kuopio were earlier found to reflect large air pollution events associated with transport of smoke plumes from fires in Russia to Finland (Portin et al., 2012; Mielonen et al., 2011). The contribution of BB emissions was clearly distinguishable against “background” conditions in Kuopio, particularly because the air pollution level there is typically very low. Although the city of Kuopio has several sites for PM₁₀ measurements, only one site (Maaherrankatu) provided data from both CO and PM₁₀ measurements; therefore, only the data from this site were used for quantitative evaluation of our model performance.

The observational data were averaged on a daily basis (the days were defined in UTC) and matched to the daily mean simulated concentrations from grid cells covering the locations of the stations. The observational (or simulated) data for the selected sites in the Moscow region for a given day were combined by averaging.

We also evaluated our simulations against aerosol optical depth (AOD) retrieved from MODIS measurements onboard the AQUA and TERRA satellites; the AOD data (Remer et al., 2005; Levy et al., 2010) with the spatial resolution of $1^\circ \times 1^\circ$ were obtained as the L3 MYD08_D3/MOD08_D3 data product from the NASA Giovanni-Interactive Visualization and Analysis system (<http://daac.gsfc.nasa.gov/giovanni/>). The MODIS AOD daily data were matched to the simulated AOD values re-gridded to the $1^\circ \times 1^\circ$ grid and averaged over the period from 10 to 14 h of local solar time (that is, over the period of daytime satellite overpasses). The same measurement data were introduced after additional spatial and temporal interpolation (Konovalov et al., 2011) into the TUV model, which (as noted above) was used to calculate the photolysis rates in CHIMERE.

2.7 Optimization of fire emissions

We calibrated the fire emissions by estimating the correction factor, F_α , involved in the relationship between FRP and the emissions (see Eqs. 3 and 4). Different estimates of F_α were derived independently from CO and PM₁₀ measurements by minimizing the following cost function, J :

$$J = \sum_{i=1}^{N_d} \theta^i (V_m^i - V_o^i - \Delta)^2, \quad (6)$$

where V_m and V_o are the modeled and observed daily concentrations of CO or PM₁₀, i is the index of a day, N_d is the total number of days in the period considered, θ_i is the operator equal to unity for days affected by fires (here, those were the days when the relative contribution of fire emissions to the simulated CO concentration exceeded 10 %) and zero otherwise, and Δ is the bias which was estimated as the mean difference between measurements and simulations on days

featuring “background” air pollution conditions (i.e., when θ_i was set to be zero).

The initial estimate of F_α was derived under the assumption of linear dependence of V_m on F_α , from results of “twin” simulations performed with $F_\alpha = 0$ and $F_\alpha = 1$. To achieve higher accuracy in the case when the estimation of F_α involved aerosol data from VBS simulations, the estimation procedure was re-iterated using a model run with F_α derived from the initial twin experiment. Otherwise (for the cases when the estimate of F_α was obtained either from CO data or using the “standard” aerosol scheme), the additional iteration was not necessary because the nonlinearity of a relationship between fire emissions and aerosol concentrations was negligible (similarly to the cases discussed in Konovalov et al., 2011 and Konovalov et al., 2014). The uncertainty in F_α was estimated from the results of the Monte-Carlo experiment involving bootstrapping of the differences between the optimized simulations and the measurements similar to Konovalov et al. (2014), except that possible uncertainties in emission factors were not explicitly taken into account in the Monte-Carlo experiment carried out in this study. Accordingly, the uncertainty in the estimates of F_α reported below reflects the uncertainty of the product of α and β^s (see Eq. 3), rather than the uncertainty in α alone.

In addition to the estimation of F_α by using ground based measurements, a similar procedure was used to derive estimates of F_α from satellite (MODIS) AOD measurements. The AOD-measurement-based values of F_α were used to obtain the “top-down” estimates of total BB aerosol emissions in the study region (see Sect. 3.4). In this case, the cost function J was formulated in the same way as in Konovalov et al. (2014):

$$J = \sum_{j=1}^{N_d} \sum_{i=1}^{N_c} \theta^{ij} (V_m^{ij} - V_o^{ij} - \Delta^{ij})^2, \quad (7)$$

where V_m and V_o are the simulated and observed AOD values for each grid cell, i , and day, j , of our model domain, N_c is the total number of grid cells in the model domain, and θ^{ij} is the selection operator taken to be unity when the relative contribution of fire emissions to the simulated AOD exceeds 10 % and zero otherwise. Estimation of the bias, Δ , in our AOD simulations was the same as in Konovalov et al. (2014), except that here, instead of averaging the differences between the simulated and measured data within a “moving window” covering 15 consecutive days, the averaging was performed over the whole period of the study (because otherwise the number of data points with $\theta^{ij} = 0$ used for estimating of the bias in the situation considered in this study was too small).

2.8 Configuration and scenarios of simulations

To be able to efficiently isolate direct effects caused by changes in the aerosol scheme on the evolution of BB aerosol from any less direct effects involving possible interference of

BB and other types of aerosol, our simulations included two stages. First, we carried out “background” simulations (labelled below as “BGR”) without fire emissions but with all the other assumed aerosol sources (such as anthropogenic, dust and biogenic emissions) and with boundary conditions from the LMDz-INCA global model (see Sect. 2.2). Taking into account that the VBS scheme had not ever been used and evaluated in simulations of aerosol evolution in Russia, we opted to simulate the background conditions by using the standard aerosol scheme. Second, the evolution of BB aerosol and associated gas species was simulated by running CHIMERE with fire emissions but without emissions from the other sources and with zero boundary conditions. Finally, concentrations of aerosol and gas species were calculated as the sum of the outputs from these two model runs.

When specifying this configuration for our simulations, we implied that the impact of fire emissions of aerosols and gases outside of the model domain on the result of our analysis was small. We took into account that our study region covers the locations of major fires in Europe and Kazakhstan during the exceptional period considered (see, e.g., Konovalov et al., 2011; Witte et al., 2011; Huijnen et al., 2012), while anti-cyclonic circulation hampered the exchange of air with the surrounding regions. The results of our simulations (see Section 3.1) confirm that the fire emissions taken into account in our simulations were indeed the major driver of the observed variability of the atmospheric chemical composition in the region and period considered in this study. Furthermore, taking into account that according to both our simulations and an independent analysis (see, e.g., Witte et al., 2011) air pollution levels over the study region in the period of intense fires were mostly determined by BB emissions, we assumed that the impact of possible interaction of BB and other emissions on the results of this study is insignificant. The configuration of our numerical experiments also implies that the POA, as well as SOA and SVOCs originating from fires are not interacting with other types of aerosol. This may not be exactly true, but presently there are no available parameterizations that could be used to describe and evaluate such interactions.

We also assumed that contribution of secondary inorganic aerosol compounds to total BB aerosol mass in the case considered was negligible and thus could be disregarded. Indeed, there are numerous observations from different regions of the world, which indicate that inorganic compounds (including water-soluble ions associated with secondary inorganic aerosol) typically constitute only a minor mass fraction ($\sim 10\%$ and less) of both fine and coarse BB aerosol particles, while POM (including OC and associated hydrogen, oxygen and nitrogen atoms) provides the predominant contribution ($\sim 80\%$) to particulate matter originating from fire (see, e.g., Reid et al., 2005a; Alves et al., 2010, 2011; Martin et al., 2010; Artaxo et al., 2013, and references therein). Consistent with our assumption, Popovicheva et al. (2014) found that the ratio of the mass concentration of inorganic

ions (sulfates, ammonium and potassium) to that of OC in aerosol observed in Moscow on several “smoky” days summer 2010 was about 0.12; assuming that the POM to OC ratio was about 2, this observation suggests that the secondary inorganic aerosol contribution to the aerosol mass concentration was much less than 10%. In addition, the measurements of submicron aerosol composition in a boreal forest in Finland during episodes of transport of BB smoke from Russian fires in July 2010 (Corrigan et al., 2013) show that the POM fraction was, on average, more than a factor of three larger than that of inorganic ions.

The results of a test run, in which we took into account all aerosol sources at once (and, consequently, all aerosol was assumed to be internally mixed) supported the validity of the above assumptions: in particular, the (calculated) mass fraction of secondary inorganic aerosol associated with fire emissions was found to be typically less than 2%, and there was no significant difference between the PM_{10} concentrations calculated assuming internal or external mixing (in the sense explained above).

We considered several model scenarios with fire emissions. Quantitative results are presented below (see Section 3) for six main scenarios; some other (test) simulations are briefly discussed. The scenario labels (used below both in the text and in the figures) and corresponding parameter settings are listed in Table 3. Specifically, along with the baseline “standard” scenario (labeled as “STN”) in which the BB aerosol evolution was simulated with the standard aerosol scheme (see Section 2.3), we designed five “VBS” scenarios in order to examine the sensitivity of our model results to different assumptions or uncertainties associated with the representation of OA processes in our model, as well as to assess the relative importance of the dilution process. Specifically, the scenarios “VBS-1” and “VBS-2” are based on the same multi-generation oxidation scheme suggested by Grieshop et al. (2009b), but involve different types of volatility distributions (“A” and “B”, respectively; see Table 1) and, accordingly, address the large uncertainty of the volatility estimates obtained by May et al. (2013). The scenario “VBS-3” is based on the modified multi-generation oxidation scheme (see Section 2.4.3) combining the representation of the functionalization process according to Grieshop et al. (2009b) and the representations of the fragmentation and condensed-phase processes according to Shrivastava et al. (2013, 2015). The scenario “VBS-4” involves a single-generation oxidation scheme (see Section 2.4.4), which was implemented in our model following Jathar et al. (2014). Finally, the scenario “VBS-5” addresses a hypothetical situation, in which there is no formation of SOA from the oxidation of SVOCs. Note that similarly to the scenario “VBS-2”, the scenarios “VBS-3” and “VBS-4” involve the volatility distribution “B”, which favors evaporation of a larger fraction of POA and therefore provides more organic material for gas-phase oxidation and eventual SOA formation than the volatility distribution “A”. Therefore, these scenarios are meant to provide the up-

per limits for SOA formation under the respective assumptions regarding gas-phase and condensed-phase processes. Note also that although the dilution experiment results by May et al. (2013) did not yield a unique value of the accommodation coefficient, we present here only the results obtained with the most probable (according to May et al., 2013) value of γ ($\gamma = 1.0$). An additional simulation was made with $\gamma = 0.1$, but since its results were found to be very similar to those obtained with $\gamma = 1.0$, they are not reported here.

The simulations that took into account emissions from fires were made using the optimal estimates of the correction factor, F_α , for BB emissions (see Eq. 3 and 4 and Sect. 2.7). The values of F_α applied to the emissions of all gaseous species were derived from CO measurements in Moscow combined with the simulations under the scenarios “STN” and “BGR” (note that gaseous species behave almost identically with any “fire” scenario considered here, since the differences between the scenarios are associated only with changes in the aerosol module). However, the values of F_α for aerosol species were optimized for each scenario independently. In doing so, we tried to isolate the effects associated with uncertainties in fire emissions from those due to inaccuracies in the representation of aerosol processes. Indeed, if the emissions were, for example, systematically overestimated, a simulation with a “perfect” aerosol module would be positively biased; in contrast, a simulation where actual SOA sources were missing could yield much better agreement with the aerosol mass concentration measurements. Therefore, evaluation of different simulations against measurements could easily prompt an incorrect conclusion regarding the model performance, unless the emissions were known to be sufficiently accurate. The idea of our analysis was therefore to adjust BB aerosol emissions to PM_{10} measurements in Moscow and then to test whether the simulations can reproduce the observed differences between PM_{10} concentrations in Moscow and Kuopio (see Sect. 3.1). A perfect simulation would be expected to yield good agreement with the measurements in both cities, while an imperfect one would likely be biased in Kuopio. Note, however, that this kind of analysis does not allow us to recognize a hypothetical situation (which is, in our opinion, rather unlikely) where the biases in the simulated aerosol evolution on its way from sources to Moscow and from Moscow to Kuopio would completely compensate each other. To reduce the risk of an incorrect conclusion, we evaluated our simulations against satellite AOD measurements (see Sect. 3.2).

3 Results

3.1 Near-surface concentrations

We focus our analysis on the air pollution events observed in the city of Kuopio (Finland) on 29 July and 8 August (Portin et al., 2012). Figure 2 demonstrates our model domains and

shows “snapshots” of the simulated distributions of CO emitted by fires not only on these days but also on the preceding days (28 July and 7 August). Our simulations demonstrate that, in each episode, the smoke that appeared over Kuopio had been transported in the north-east direction from a region around Moscow, where the largest fires had occurred (Konovalov et al., 2011). As an illustration of sources of the smoke plumes, Fig. 2 also shows the spatial distributions of CO emissions from fires on 28 July and 7 August. We estimate that the age of smoke in the plumes passing over Kuopio was mostly in the range from 1 to 3 days. This estimate is in line with results of back-trajectory analyses (Portin et al., 2012). Note that CO behaved almost identically in all of the simulation scenarios in which the BB emissions were taken into account; therefore, for clarity, the evolution of CO from fires is presented here only for the STN scenario (that is, with the scenario using the standard version of CHIMERE).

Figure 3 shows the evolution of CO in the Moscow region and in Kuopio according to both measurements and simulations. The simulations taking into account fire emissions were made with the optimal estimate of F_α (derived from CO measurements in Moscow and applied to emissions of all gaseous species in all of the simulations discussed below) of 1.88; the uncertainty of this estimate was evaluated in terms of the geometrical SD to be 1.14. The model as well as observations demonstrate episodes of very strong enhancements of CO concentration in both Moscow (mainly in early August) and in Kuopio (in the end of July and early August). The correlation of the simulated and observed time series is considerable at both locations ($r = 0.88$ in Moscow and $r = 0.76$ in Kuopio). Note that the optimization of just one parameter of our fire emission model (see Eqs. 3 and 4) could adjust the amplitude of CO variations in Moscow, but could not be responsible for the rather strong correlation between the simulations and measurements, if our fire emission data were completely wrong. Most importantly, our simulations are capable of reproducing the major features of the observed CO evolution at a location about a thousand kilometers away from the source regions; in particular, the model and the measurements demonstrate a good agreement of peak CO concentrations on 29 July and 8 August. The differences between the simulated and observed CO concentrations in Kuopio can partly be due to the fact that this city was situated at the edge of the smoke plumes (see Fig. 2), where the concentration gradients were large and where the simulations were especially sensitive to any transport and emission errors. Note also that the rather high correlation obtained for the Kuopio site in the case of the BGR scenario ($r = 0.75$) reflects covariation of the observations with a contribution of anthropogenic pollution transported from Russia to Finland to the CO level in Kuopio; however, the transport of anthropogenic CO (coinciding in space and time with the transport of CO from fires) can explain only a minor part of the observed CO variations. On the whole, the results shown in Fig. 3 indicate that both fire emissions and transport processes during the

study period are simulated rather adequately by our modeling system, although not perfectly.

Time series of PM_{10} concentrations from simulations performed with the standard version of CHIMERE (that is, with the STN scenario) and with the VBS-3 scenario (which was supposed to provide the most realistic representation of the BB aerosol ageing) are shown in Figure 4 in comparison with corresponding measurement data.

In spite of the considerable differences between the representations of aerosol processes in the different aerosol schemes, simulations for the STN and all of the VBS scenarios demonstrate very similar performance when compared to the Moscow observational data (see Fig. 4a and Table 4), mainly because these data have been used to adjust the emissions (as explained in Sect. 2.7). However, major differences between the different simulation scenarios become evident when the simulated data are compared to the measurements in Kuopio (see Fig. 4b and Table 5). Specifically, the VBS version of the model (for the VBS-3 scenario) predicts at least 70 % large contribution of fire emissions to PM_{10} concentration on both 29 July and 8 August, and enables achieving much better agreement of the simulations with the measurements on these remarkable days than the standard version. The differences between the performance statistics calculated for the whole time series of the VBS and STN simulations are not quite unequivocal: on the one hand, the use of the VBS scheme instead of the standard scheme is associated with a decrease (from 7.3 to 6.3 $\mu\text{g m}^{-3}$) of the root mean square error (RMSE) and with improving agreement between the mean values of the observed and simulated PM_{10} ; but, on the other hand, the VBS-3 scenario yields a slightly lower correlation coefficient ($r = 0.89$) than the STN scenario ($r = 0.91$). The decrease in the correlation coefficient is partly due to a strong overestimation of PM_{10} in the VBS simulation (similar to an overestimation of CO in the STN simulation) on 9 August.

Similar to the VBS-3 scenario, the other scenarios with the VBS scheme involving the multi-stage oxidation parameterization yield considerably better agreement of simulations with measurements in Kuopio, compared to the STN scenario. The time series of PM_{10} concentrations from these and other scenarios considered (except for the scenario VBS-3 presented in Fig. 4b) are shown in Fig. 5. As it could be expected, the scenario “VBS-2” (under which the increase of the mass of S-SOA species was not limited by the fragmentation process as in the scenario “VBS-3”) yielded the largest PM_{10} concentrations, although the difference with the concentrations (and statistics) obtained with the scenario “VBS-3” is not large. A difference (although not very considerable) between the results of the scenarios “VBS-2” and “VBS-1” indicates that assuming a larger fraction of POA species available for gas-phase oxidation (at least, within the considered volatility range) favored formation of more SOA in the situation considered. The PM_{10} concentrations obtained for the VBS-4 scenario involving a single-generation oxidation

scheme were significantly smaller compared to those calculated for the VBS scenarios with the multi-generation schemes. Apparently, the main reason for this difference is the fact that the parameterization by Jathar et al. (2014) assumes effectively (after sufficiently long oxidation) much smaller mass yields of the S-SOA species from oxidation of POA than our VBS schemes based on Grieshop et al. (2009b).

Note again that the simulations presented in Fig. 5 were made using estimates of F_{α} adjusted independently for each scenario. This adjustment partly explains why the scenario “VBS-5” (under which a major fraction of initial particle emissions is expected to be irreversibly lost due to evaporation in the absence of SOA production from SVOCs) yields almost the same results as the scenario “STN”. Indeed, the optimal F_{α} value for the VBS-5 scenario is 50 % larger than that for the STN scenario, and this fact indicates (taking into account the difference between the emission factors for POA and OC in accordance with Eq. 1) that about 44 % of primary POA species (mostly from the 6th and 7th volatility classes) already evaporated due to dilution (i.e., due to decrease in ambient C_{OA} levels) before they reached the monitoring sites in the Moscow regions. Further evaporation (mostly from the 5th volatility class) was relatively small and was partly offset by stronger production of SOA from oxidation of VOCs in the VBS scheme than in the standard aerosol scheme (as demonstrated below in Sect. 3.3). Unlike the VBS-5 scenario, the other VBS scenarios yield optimal F_{α} values that are similar to that for the STN scenario. These estimates indicate that evaporation of POA species within the source region was effectively counterbalanced by SOA production.

To quantify the changes of aerosol concentrations relative to the concentration of CO (which can be regarded as a chemically passive tracer on the time scales considered in this study) in BB plumes, it is convenient to consider the normalized excess mixing ratio (NEMR) (similar, e.g. to Vakkari et al., 2014). In our case, NEMR can be defined as the ratio of ΔPM_{10} to ΔCO , where Δ denotes the “excess” concentration contributed by fires.

Figure 6 illustrates the spatial distributions of NEMR in the smoke plumes transported from Russia to Finland on 29 July and 8 August according to our simulations for the STN and VBS-3 scenarios. Evidently, the NEMR distributions obtained for these two scenarios are strikingly different. In particular, while NEMR calculated with the standard version of CHIMERE tends to decrease (apparently due to mainly aerosol deposition) as the smoke is transported away from the major fires that occurred south-east from Moscow (see Fig. 2e and f), the VBS version enables net production of aerosol during the same smoke transport events. Therefore, our simulations indicate a major role of oxidation processes, which dominate over evaporation of primary SVOCs due to smoke dilution and over dry deposition almost everywhere. As one of the spectacular manifestations of the fundamental differences between the representations of aerosol pro-

cesses in the standard and VBS schemes, the NEMR values in the grid cell corresponding to Kuopio are almost two times larger in the VBS simulation than in the standard simulation. In general, the NEMR values are largest at the edges of the plumes, where the aerosol is likely to be more “aged” and more diluted. The increase of NEMR in the central (most dense) part of the plumes is hampered by relatively slow evaporation of POA species and also by slowing-down of SVOC oxidation due to attenuation of photolysis rates by BB smoke (note a “valley” of NEMR local minimums in Fig. 6d along a direct (imaginary) line connecting Moscow and Kuopio; this “valley” coincides with the location of the thickest smoke (see Fig. 2d)). The effect of attenuation of photolysis rates by BB smoke on SOA formation in the situation considered is analyzed in detail in Konovalov et al. (2015).

Note that the excess concentrations, ΔPM_{10} and ΔCO , which were used to calculate the NEMR values shown in Fig. 6 were simply PM_{10} and CO concentrations obtained from the model runs where fire emissions were the only sources of aerosol and gases (see Sect. 2.8). In order to characterize the NEMR values over the whole study period independently both in the observations and simulations, we first estimated the ΔPM_{10} and ΔCO values as the difference between the concentrations with all the sources (either observed or calculated by combining results of the “background” and respective “fire” runs as explained in Sect. 2.8) and the corresponding average concentrations over the “background” days when the contribution of fires to CO concentration was smaller (according to our simulations) than 10%. Second, we evaluated the slope of a linear fit to the relationship between ΔPM_{10} and ΔCO values defined in this way for each “smoky” day (that is, when the contribution of fires to CO concentration exceeded 10%). The “fitted” NEMR values (denoted below as $[\Delta\text{PM}_{10}/\Delta\text{CO}]_{\text{fit}}$) were calculated independently for the Moscow and Kuopio sites, both with the measurement and simulation data (see Fig. 7 and Tables 4 and 5).

Comparison of the $[\Delta\text{PM}_{10}/\Delta\text{CO}]_{\text{fit}}$ values calculated using measurement data reveals that $[\Delta\text{PM}_{10}/\Delta\text{CO}]_{\text{fit}}$ is more than two times larger in Kuopio (0.18 g g^{-1}) than in Moscow (0.07 g g^{-1}). We regard this fact (which was not noted in earlier publications) as strong observational evidence of SOA formation in BB plumes during their transport from the Moscow region to Kuopio. In order to make sure that the major difference between the “observed” $[\Delta\text{PM}_{10}/\Delta\text{CO}]_{\text{fit}}$ values for Moscow and Kuopio is not an artifact of averaging of CO and PM_{10} measurements from 4 different monitoring stations in Moscow and/or a result of a technical failure of one of the monitors, we additionally evaluated $[\Delta\text{PM}_{10}/\Delta\text{CO}]_{\text{fit}}$ for each of the monitoring sites separately. The following values – 0.08, 0.06, 0.02, and 0.09 g g^{-1} – were found with the data from the “Zelenograd”, “MGU”, “Pavlovskii Posad”, and “Kozhuhovo” monitoring stations, respectively. All these values (in spite of their big differences, which probably reflect regional vari-

ability of ΔPM_{10} and ΔCO ratios due to varying emissions factors for different fires) are considerably smaller than the $[\Delta\text{PM}_{10}/\Delta\text{CO}]_{\text{fit}}$ value obtained from the measurements in the city of Kuopio.

In line with the results shown in Fig. 6a and c, the CHIMERE standard version (which yields little SOA in BB plumes) failed to explain the increase of NEMR in Kuopio predicting a much smaller relative increase in the aerosol concentration: with this version $[\Delta\text{PM}_{10}/\Delta\text{CO}]_{\text{fit}}$ is calculated to be only 26% larger in Kuopio than in Moscow. Probably, this change mostly reflects the daily variability of the NEMR values and background concentrations. Note that the available measurement data do not allow us to evaluate temporal variability of the background concentrations of PM_{10} and CO in the real atmosphere without using corresponding simulations. Therefore, our interpretation of the large difference between the “observed” values of $[\Delta\text{PM}_{10}/\Delta\text{CO}]_{\text{fit}}$ in Moscow and Kuopio is, to some extent, dependent on reliability of our simulations of the background concentrations. Uncertainties in such simulations may, in particular, be due to effects of fires (and associated air pollution) on mesoscale transport processes; such effects have not been addressed in our model.

The NEMR value for the VBS-3 scenario was found to be considerably (46%) higher than that for the STN scenario. This difference enabled the VBS-3 simulation to reproduce the observed changes in the NEMR values within the range of statistical uncertainties. Using the VBS scheme with the other scenarios (except for the VBS-5 scenario) also resulted in a better agreement of the $[\Delta\text{PM}_{10}/\Delta\text{CO}]_{\text{fit}}$ values obtained from simulations and measurements (see Table 5).

In addition to the simulations discussed above we performed a test model run under a modified VBS-2 scenario in which the second and further stages of POA oxidation were completely switched off (that is, there was no oxidation of S-SOA-f). Not surprisingly, the NEMR ($[\Delta\text{PM}_{10}/\Delta\text{CO}]_{\text{fit}}$) value obtained with this simulation was considerably ($\sim 30\%$) lower than that with the original VBS-2 simulation (0.11 vs. 0.15 g g^{-1}). However, it was still considerably larger than the NEMR value for the VBS-5 scenario (0.07) in which S-SOA formation was switched off completely. These results suggest that about a half of the aerosol mass enhancement on the way of the BB plumes from Moscow to Kuopio was due to the first stage of POA oxidation, which is best constrained by laboratory measurements (Grieshop et al., 2009a). Note that, unlike Shrivastava et al. (2015), we found that the condensed-phase transformation processes had only a small impact on the simulated OA evolution: specifically, an additional model run under the VBS-3 scenario, but without the condensed-phase transformation gave only slightly smaller NEMR (within 5%) than the “original” VBS-3 scenario. Probably, the sensitivity of our simulations to the condensed-phase processes is much smaller in our case than in the global scale simulations by Shrivastava et al. (2015), because OA concentration was

strongly reduced in plume outflow far away from sources in the simulations by Shrivastava et al. (2015) during transport and dilution, and that favored evaporation of S-SOA, while the much higher OA concentrations in our mesoscale simulations prompted a strong depletion of the gas-phase concentrations of S-SOA almost irrespectively of the assumed rate of the condensed-phase transformation.

3.2 Aerosol optical depth

Figure 8 presents the spatial distribution of AOD on 8 August 2010 according to simulations performed with the STN and VBS-3 scenarios in comparison with the corresponding MODIS measurement data. A very large BB plume reaching Kuopio is clearly visible both in the model and measurements data, although there are also considerable differences between the measurements and simulations. Visually, the differences are largest between the measurement data and the simulations made with the STN scenario: clearly, the standard model strongly underestimates AOD in many locations, including both Moscow and Kuopio. The differences between the measurements and the VBS-3 simulations are smaller, and much better agreement between them is evident compared to the results for the STN scenario. Interestingly, the VBS method gives significantly larger AOD than the standard method even in the source region, although the corresponding near-surface PM_{10} concentrations predicted with the methods are very similar. In fact, we found that the VBS-3 simulation predicts a larger contribution of SOA to OA concentrations at higher altitudes (in the Moscow region) than to near-surface concentrations; this can be due to both a larger typical “age” of OA situated at higher altitudes and lower temperatures leading to more condensation of SVOCs.

Time series of daily AOD values averaged over the study region are shown in Fig. 9. Averaging the AOD data over the whole domain is expected to minimize the contribution of random errors in the simulations and measurements to the respective time series. Obviously, the standard simulation strongly underestimates AOD. The simulation with the VBS-3 scenario typically predicts a much larger (about a factor of 2, on the average) contribution of BB aerosol to AOD, compared to the simulation with the STN scenario. Accordingly, the use of the VBS method instead of the standard one enables much better overall agreement of simulations with the measurements, although a negative bias in the simulated data is not completely eliminated. A part of this bias may, in principle, be due to uncertainty ($\sim 20\%$) in the estimate of the mass extinction efficiency employed in this study to convert the simulated aerosol mass column concentration into AOD (see also Sect. 2.2).

It should be kept in mind that not only are our simulations imperfect, but that the AOD measurement data that we use here for comparison can also contain considerable uncertainties. In particular, van Donkelaar et al. (2011) found that the relative error of the “operational” AOD retrievals at the

10 km \times 10 km resolution in the Moscow region between 26 July and 20 August 2010 was on average about 20 %, and that a part of this error was due to incorrect identification of some aerosol as cloud. Although the uncertainties in the level 3 data product (at the $1^\circ \times 1^\circ$ resolution) used in this study are likely to be smaller than those in the operational retrievals, spatial averaging could hardly diminish probable systematic uncertainties associated with the cloud screening algorithm. Based on the analysis by van Donkelaar et al. (2011), it seems safe to assume that those systematic uncertainties on average do not exceed 10 %; however, they may occasionally be much larger in grid cells where AOD is approaching a value of 5 (since the standard MODIS algorithm removes any retrieved AOD greater than this value).

3.3 Aerosol composition

Although our simulations based on a simple VBS scheme do not allow distinguishing between different chemical compounds contributing to OA matter, they still can provide some useful insight into the changes of aerosol composition caused by absorption/desorption and oxidation processes involving SVOC (that is, by the processes that are largely disregarded in the framework of the conventional approach to OA modelling). Figure 10 compares the speciation of BB aerosol according to our simulations made with the STN and VBS-3 scenarios. Specifically, we consider near-surface data from two model grid cells covering the city centers of Moscow and Kuopio. The Moscow and Kuopio data correspond to 18:00 UTC on 7 and 8 August, respectively: we expect that the differences between these data qualitatively reflect changes in the BB aerosol composition as a result of aerosol ageing during transport of BB plumes between the source and receptor regions considered.

Obviously, the results obtained with the standard and VBS schemes are profoundly different. In particular, while the STN simulation predicts that more than 90 % of BB aerosol composition is determined by POA species both in Moscow and in Kuopio, the VBS-scenario indicates a large contribution of secondary semi-volatile and non-volatile organic species (S-SOA and NVSOA) originating from oxidation of POA. As expected, the combined fraction of S-SOA and NVSOA species is much larger in Kuopio (69 %) than in Moscow (35.5 %), with the POA fraction shrinking from 50.8 % in Moscow to merely 12.9 % in Kuopio. Considerable fractions of NVSOA and S-SOA in Moscow indicate that oxidation processes were rapid enough to already transform the composition of BB aerosol on its way (typically having taken several hours) from the fire spots to Moscow. It is noteworthy that according to our simulation almost all S-SOA species in the particle phase could be transformed into NVSOA species in Kuopio; but it should also be noted that an additional test run in which possible condensed-phase transformation processes were not taken into account (see also Sect. 3.1) showed almost the same contribution of SOA

species to aerosol composition both in Moscow and Kuopio¹⁴⁸⁵ as the VBS-3 run.

Compared to the standard scheme, the VBS scheme yields also a larger fraction of SOA (V-SOA) formed from oxidation of volatile (traditional) precursors, but the contribution of V-SOA (which was supposed not to be affected by the condensed-phase transformation in our simulations) still remains minor even in the aged plumes. Both scenarios predict that the black carbon (BC) fraction is, expectedly, also small at both locations and is about 6 % or less. For comparison, the average OC/BC ratio observed in Moscow by Popovicheva¹⁴⁹⁵ et al. (2014) on smoky days in August 2010 was 14.2; assuming that the ratio of POM to OC was 1.8 as in our simulations, this observation indicates that the mass fraction of BC was slightly less than 4 %. It is noteworthy that the BC fraction in Kuopio is considerably smaller in the VBS simulation than in the standard model run. This is a result of increasing the total mass of aerosol particles due to condensation of oxidized material. Data of BC measurements in Kuopio were available only from the Puijo tower atmospheric measurement station (Leskinen et al., 2009; Portin et al., 2012), which unfortunately did not provide simultaneous accurate measurements of PM₁₀ or OC. However, if we assume that the contribution of BB aerosol to PM₁₀ on the “smoky” days (29 July and 8 August) at the Puijo site was the same as that at the Maaherankatu site, we can estimate (using the data from Table 1 in Portin et al., 2012) that the mass fraction of BC aerosol was about 2 %. Obviously, using such an “approximate” estimate does not enable us to make any firm conclusion about the relative accuracy of our VBS-3 or STN simulations with regard to the BC fraction, but nonetheless it indicates that the BC¹⁵¹⁵ fraction in BB aerosol in Kuopio could be overpredicted by the standard model.

3.4 Top-down estimates of BB aerosol emissions

Obtaining top-down estimates (that is, estimates constrained by atmospheric measurements) of emissions of aerosols (as well as gaseous species) by using the inverse modelling approach (see, e.g., Enting, 2002; Zhang et al., 2005; Dubovik et al., 2008; Huneus et al., 2012; Xu et al., 2013) is aimed at validation and improvement of “bottom-up” emission inventories and at advancing our general knowledge of the emission processes. As noted in the introduction, the models employed in inverse modelling studies have conventionally simulated BB aerosol under the assumption that it consists of non-volatile material. Here we examined, in particular, whether or not top-down estimates of BB emissions could change significantly if this assumption was relaxed in accordance with the absorptive partitioning theory.

We obtained top-down estimates of total emissions of aerosol from fires in the study region during the period from 1 July to 31 August 2010 by using the MODIS AOD measurements and the correction factor (F_α) values estimated for the period covered by our simulations (from 15 July to

20 August). The F_α estimates are applied to the extended period, taking into account that fire emissions in the first half of July and the second half of August were relatively very small, in order to compare our emission estimates with available monthly data of bottom-up inventories. Our emission estimates, along with the corresponding estimates of the correction factor F_α for the same modelling scenarios as those discussed above (except for the estimates for the unrealistic scenario “VBS-5”), are presented in Fig. 11. The emission estimates are shown in comparison with the data from the bottom-up fire emission inventories, such as GFED3.1 and GFASv1.0, for emissions of total particulate matter (TPM), whereas the estimates of F_α derived from satellite measurements are presented along with the corresponding estimates obtained from ground-based measurements (see also Table 4). The estimates for the scenario VBS-5 are omitted from these figures, because they turn out to be much larger (as could be expected) than those for all the other scenarios and are clearly unrealistic (specifically, the total aerosol emissions were ~ 1.8 Tg according to the VBS-5 scenario, compared to ~ 1.3 Tg for the STN scenario). The much larger estimate for the VBS-5 scenario (relative to the estimates for the both STN scenario and the other VBS scenarios) is indicative of the major roles of both SOA formation and dilution of POA in the study region during the period of intense fires. Note that the uncertainties of the different estimates of the top-down emissions and the correction factors are not statistically independent. The emission estimates for the VBS scenarios are reported assuming the ambient level of OA concentration (C_{OA}) during the emission factor measurements to be 10 mg m^{-3} (see Sect. 2.4.1); under this assumption, the total POA emissions are about 20 % larger. Optimization of F_α is expected to compensate possible uncertainties in the POA emission factors. Note again that the experimental data for the OA emission factors can depend (as argued, e.g., by Robinson et al., 2007) on C_{OA} and ambient temperature, which are unfortunately not reported in the literature together with the emission factor estimates.

It can be seen that (1) the BB aerosol emission estimate obtained using the standard model (1.26 Tg TPM) is about 30 % larger than the corresponding estimate based on using the VBS approach with the VBS-3 scenario (0.96 Tg TPM), (2) the estimates for the scenarios “VBS-1” and “VBS-2” are also considerably smaller than the estimate for the STN scenario, (3) all estimates obtained using the VBS framework (except for the estimate for the unrealistic VBS-5 scenario) show better agreement with both the GFASv1.0 and GFED3.1 data than the estimate for the STN scenario. Another important result is that the optimal estimates of F_α (and the corresponding top-down emission estimates) derived from the AOD measurements for all VBS scenarios presented in Fig. 11 are consistent (within the range uncertainty) with the corresponding estimates derived from local near-surface monitoring data, while this is obviously not the case with the estimate obtained by using the standard approach.

The inconsistency of the estimates based on the independent data means that they fail to pass the cross-validation, which is indicative of major deficiencies of simulations based on the standard approach. On the other hand, the fact that the estimates of F_{α} derived from satellite and ground-based measurements are consistent provides strong evidence in favor of the reliability of our top-down emission estimates obtained with the VBS framework. Regarding the remaining differences between our emission estimates and the corresponding data of the GFED3.1 inventory, it can be noted that there is evidence (e.g., Fokeeva et al., 2011; Konovalov et al., 2011; Krol et al., 2013) that the GFED3.1 inventory strongly underestimated the CO emissions from the 2010 Russian fires; it seems thus reasonable to expect that the TPM emissions were also underestimated by this inventory.

4 Discussion

In this section, we summarize our findings presented above and discuss their possible implications for other modeling studies of BB aerosol sources and evolution. First, although this is a modeling study, it is worth noting that our analysis revealed interesting observational evidence of strong formation of SOA in BB plumes at the mesoscale. Specifically, the normalized excess mixing ratio (NEMR) of BB aerosol was found to increase, on the average, by more than a factor of two while BB plumes were transported from the source region around Moscow to the city of Kuopio, Finland (about 1000 km from Moscow). Although the possibility of considerable SOA formation as a result of photochemical oxidation of BB emissions has been demonstrated in smog chamber experiments (Grieshop et al., 2009b; Hennigan et al., 2011; Heringa et al., 2011; Ortega et al., 2013), different field studies reported rather inconsistent findings. For example, fast (within several hours) and strong SOA formation events (associated with an increase of NEMR by a factor of two and more) in savannas were reported by Yokelson et al. (2009) and Vakkari et al. (2014). However, Akagi et al. (2012) reported a net increase in the OA NEMR of only about 20% over four hours in the case of chaparral fires in California, and Jolleys et al. (2015) observed higher NEMR values closer to source than in aged plumes from Canadian fires. Overall, the available laboratory studies and atmospheric observations suggest that the SOA formation in the real atmosphere can be strongly influenced by the type of fuel and conditions of burning, as well as by the atmospheric conditions of BB aerosol evolution. In this respect, our study indicates that an important source of SOA in the atmosphere can be associated, specifically, with wildfires in Russian boreal forests which contain about 25% of global terrestrial biomass (Conard et al., 2002). One reason for this strong SOA production may be the high terpenoid content of the boreal forest fuels. Therefore, we believe that this case study

can provide a strong impetus for further studies and evaluation of SOA originating from wildfires in Russia.

Second, we found that simulations of BB aerosol evolution by using a “conventional” SOA scheme (which disregards for formation of SOA from oxidation of POA and assumes that OA particles are composed of non-volatile material) could not explain the observed enhancement of the NEMR ratio. Thus our results indicate that the use of the conventional OA modeling methods in studies of BB aerosol mesoscale evolution can result in considerable negative biases in the simulated aerosol concentrations; probably, such biases can explain at least a part of the earlier reported systematic discrepancies between BB aerosol concentrations from modeling and measurements (Wang et al., 2006; Strand et al., 2012). Note that, in general, our findings concerning potential deficiencies of the “conventional” approach to OA modeling are in line with the findings of several earlier studies (e.g., Heald et al., 2005; Bessagnet et al., 2009; Hodzic et al., 2010; Zhang et al., 2013) in which chemistry transport models considerably underestimated observed concentrations of OA originating from various sources when using the conventional approach.

Third, we found that a rather good quantitative agreement between simulations and measurements could be achieved by using the VBS framework with parameter values constrained (even though rather loosely) by laboratory measurements. This is an important result, especially in view of the fact that, to the best of our knowledge, there have so far been no modeling studies focusing on examination of BB aerosol mass enhancements in the real atmosphere. Indeed, on the one hand, the period of atmospheric evolution of BB aerosol in the case considered (more than one day) significantly surpassed the duration of typical smog chamber experiments (a few hours), which were used to constrain the parameters of our VBS scheme. On the other hand, the SOA formation rate has been found to be highly variable even in laboratory measurements (see, e.g., Hennigan et al., 2011). It is also important that the results of our simulations turned out to be rather robust with respect to potentially large uncertainties in the parameterizations of OA atmospheric processing. All our simulations (except for a simulation with the “unrealistic” scenario “VBS-5”) demonstrated a better overall agreement with the measurements than the “conventional” simulations (with the STN scenario). Our results are found to be moderately sensitive to the assumptions regarding the fragmentation process and to the volatility distribution of POA species. Specifically, taking the fragmentation process into account (as in the VBS-3 scenario) decreased the NEMR value by $\sim 15\%$ with respect to the VBS-2 scenario (without fragmentation) even though fragmentation could be partly counterbalanced (in the VBS-3 simulation) by the condensed-phase transformation of oxygenated organics into non-volatile species. In contrast, a shift of the assumed POA volatility distribution toward more volatile bins resulted in the increase of the NEMR values by about $\sim 40\%$ and in

an improvement of the agreement of our simulations with the measurements (cf. results for the scenarios “VBS-1” and “VBS-2” in Table 5). These results are consistent with the findings of other available studies of OA evolution. For example, a strong impact of the fragmentation process, which counteracts functionalization and eventually hampers SOA formation, on 3-D modeling results was reported by Shrivastava et al. (2013, 2015). Also, Grieshop et al. (2009b) found that increasing the fraction of more volatile POA species increased the rate of OA enhancement in their box model (probably, because a larger fraction of volatile species means that a larger mass may be potentially gained as a result of their gas-phase oxidation). It is also noteworthy that the performance of simulations involving a single-generation oxidation scheme (as in the scenario “VBS-4”) proved to be inferior in comparison to the performance of the simulations involving a multi-generation oxidation mechanism (as in the scenarios from “VBS-1” to “VBS-3”). This is, in principle, an expected outcome, since the single-generation scheme was not designed to predict SOA formation beyond the typical time scales of the laboratory experiments that were used to fit its parameters. Overall, we believe that our results concerning the sensitivity of the simulations of BB aerosol evolution to the choice of configuration and parameter values of the VBS scheme can be helpful for planning further modeling studies of BB aerosol evolution.

Fourth, the results of our study have direct implications for inverse modeling of aerosol emissions. While previous studies providing measurement-based constraints for carbonaceous aerosol emissions (including, either explicitly or implicitly, emission from biomass burning) involved either the conventional modeling representation of SOA formation (Kononov et al., 2014) or disregarded it entirely (e.g., Zhang et al., 2005; Schutgens et al., 2012; Petrenko et al., 2012; Huneus et al., 2012; Kaiser et al., 2012), we found that taking the SOA source from oxidation of SVOCs into account could significantly affect the emission estimates. This result suggests that the findings of some earlier studies indicating that BB aerosol emissions in “bottom-up” inventories are likely underestimated (e.g., Zhang et al., 2005; Kaiser et al., 2012; Petrenko et al., 2012; Kononov et al., 2014) could, at least partly, be an artifact of “biased” representations of BB aerosol evolution in the models involved. Therefore, the adequacy of representation of SOA formation in a concrete model needs to be carefully evaluated prior to using that model for estimating BB aerosol emissions.

Fifth, we have demonstrated that important implications of taking volatility of POA species and their gas-phase oxidation into account include major changes in the composition of the aerosol particles with respect to the case where simulations follow the conventional approach to OA modeling. Our results show that the gas-phase ageing of BB aerosol is associated with replacement of POA species by SOA species, formed mostly from the oxidation of primary semi-volatile organic compounds. Specifically, according to our VBS sim-

ulations, SOA contributed more than 80 % to BB aerosol in Kuopio during an air pollution event on 8 August 2010. Oxygenated organics are likely to contain light-absorbing brown carbon (Saleh et al., 2013), are known to be more hygroscopic (Jimenez et al., 2009) and are expected to have a larger health impact, when inhaled as particles than primary organics (Stevanovic et al., 2013). Therefore, BB aerosol ageing (which obviously cannot be described adequately with the “conventional” approach) should be taken into account in climate models where the absorptivity and hygroscopicity of aerosol (providing cloud condensation nuclei) are important parameters (e.g., Andreae and Ramanathan, 2013; Andreae and Rosenfeld, 2008; Pöschl et al., 2009) as well as in air pollution models.

It should be emphasized that our numerical experiments with the VBS scheme were neither intended nor allowed us to estimate the real values of the parameters of the processes considered. Indeed, our VBS schemes provided only a very simplistic representation of the complex processes involving absorption/desorption and oxidation of organic material. For example, Donahue et al. (2012) and Murphy et al. (2012) argue that explicit accounting for changes in the O : C ratio in a VBS scheme is important for better constraining the average organic properties. An even much more complex (and potentially realistic) OA evolution scheme could involve explicit characterization of chemical and physical properties of different organic species (Lee-Taylor et al., 2015). A general problem arising with more complex schemes is the lack of sufficient laboratory or ambient measurement data needed to constrain all the parameters. On the other hand, there is always the possibility that a simplistic scheme may demonstrate good performance for a wrong reason; for example, when optimization of its parameters compensates some systematic model errors. In our case, systematic model errors may be associated, in particular, with parameters involved in the representation of OA ageing processes, such as, e.g., the branching ratios between functionalization and fragmentation, as well as with uncertainties in the POA emissions. Our model also omits formation of new OA particles (i.e., the nucleation process), which may be important at least during the initial hours of the atmospheric processing of BB smoke (e.g., Vakkari et al., 2014). Nonetheless, our results provide strong evidence that the VBS method applied in this study to a special case of modeling aerosol originating from wildfires is indeed superior to the “conventional” method.

5 Conclusions

In this study, we used the volatility basis set (VBS) framework for organic aerosol (OA) modeling to simulate the mesoscale evolution of aerosol from open biomass burning for the case of the mega-fire event that occurred in Russia in summer 2010. We modified the VBS scheme in the CHIMERE chemistry transport model by using data from

laboratory experiments aimed at studying gas-particle partitioning and oxidation processes in the mixtures of gases and aerosols emitted from biomass burning (BB). We also used standard version of CHIMERE with a “conventional” method for OA modeling, which disregards the volatility of primary OA species and the formation of secondary organic aerosol by oxidation of semi-volatile precursors. Several simulation scenarios were considered to test the sensitivity of the model output data to possible uncertainties in the parameters of the VBS scheme and to evaluate the relative roles of dilution, oxidation and fragmentation processes in the evolution of aerosol in BB plumes. Emissions of gases and particles from fires were modeled using fire radiative power (FRP) data from satellite (MODIS) measurements, and were constrained by CO and PM₁₀ air pollution monitoring data in the Moscow region.

The results of our simulations made with the VBS scheme were compared with the corresponding results obtained with the standard OA scheme in CHIMERE and with data from ground-based and satellite measurements. In particular, we evaluated our simulations with respect to the normalized excess mixing ratio (NEMR) of BB aerosol (that is the ratio of enhancements in PM₁₀ and CO concentrations) by using measurements at an air pollution monitoring site in the city of Kuopio, Finland (situated about 1000 km northwest from Moscow). Whereas the standard simulations were found to strongly underestimate the observed NEMR in Kuopio (which turned out to be more than two times larger than in Moscow, thus indicating the gain of BB aerosol mass during transport from Russia to Finland), the simulations performed using the VBS framework proved to be in much better agreement with the measurements. Similar results were obtained when evaluating our simulations against satellite AOD measurements.

Taking the semi-volatile nature of BB aerosol into account within the VBS framework was found to result in major changes in the predicted aerosol composition and to have a considerable impact on the top-down BB emission estimates derived from satellite AOD measurements by means of inverse modeling. Specifically, our VBS simulations indicated that a major part (more than 80 percent) of primary OA material in BB plumes transported from the Moscow region to Kuopio was eventually replaced by secondary oxygenated organics. The total BB aerosol emissions from the 2010 Russian fires in the region and period considered in this study are estimated to be about 30 % larger with simulations based on the “conventional” method, compared to the case when our model used the version of the VBS scheme that we consider being the most adequate. Moreover, it was found that while both satellite and ground based measurements enabled consistent constraints to aerosol emissions from the 2010 Russian fires when CHIMERE employed the VBS scheme, this was not the case when the standard aerosol scheme was used.

Future studies of BB aerosol evolution, combining modeling with laboratory and field measurements, should provide

stronger constraints to the parameters of the OA transformation processes addressed in the framework of the VBS framework, and enable further development of the VBS approach for the particular case of OA originating from open biomass burning. Further efforts are also needed towards achieving a better understanding of the possible differences between the ageing of BB aerosol from fires in different regions and climate zones and addressing these differences in chemistry transport and climate models.

Acknowledgements. This study was supported by the Russian Foundation for Basic Research (grants No. 14-05-00481 and 15-45-02516). The CHIMERE model was modified with support from the Russian Science Foundation (grant agreement No. 15-17-10024). The authors are grateful to E.G. Semutnikova for providing the Mosecomonitoring data. The authors are also grateful to the City of Kuopio for the air quality data. T.M.’s work was supported by Academy of Finland Center of Excellence Program (decision 272041).

References

- Ahmadov, R., McKeen, S. A., Robinson, A. L., Bahreini, R., Middlebrook, A. M., de Gouw, J. A., Meagher, J., Hsie, E.-Y., Edgerton, E., Shaw, S., and Trainer, M.: A volatility basis set model for summertime secondary organic aerosols over the eastern United States in 2006, *J. Geophys. Res.*, 117, D06301, doi:10.1029/2011JD016831, 2012.
- Akagi, S. K., Yokelson, R. J., Wiedinmyer, C., Alvarado, M. J., Reid, J. S., Karl, T., Crounse, J. D., and Wennberg, P. O.: Emission factors for open and domestic biomass burning for use in atmospheric models, *Atmos. Chem. Phys.*, 11, 4039–4072, doi:10.5194/acp-11-4039-2011, 2011.
- Akagi, S. K., Craven, J. S., Taylor, J. W., McMeeking, G. R., Yokelson, R. J., Burling, I. R., Urbanski, S. P., Wold, C. E., Seinfeld, J. H., Coe, H., Alvarado, M. J., and Weise, D. R.: Evolution of trace gases and particles emitted by a chaparral fire in California, *Atmos. Chem. Phys.*, 12, 1397–1421, doi:10.5194/acp-12-1397-2012, 2012.
- Alves, C. A., Gonçalves, C., Pio, C. A., Mirante, F., Caseiro, A., Tarelho, L., Freitas, M. C., and Viegas, D. X.: Smoke emissions from biomass burning in a Mediterranean shrubland, *Atmos. Environ.*, 44, 3024–3033, 2010.
- Alves, C., Vicente, A., Nunes, T., Gonçalves, C., Fernandes, A. P., Mirante, F., Tarelho, L., de la Campa, A. M. S., Querol, X., Caseiro, A., Monteiro, C., Evtyugina, M., and Pio, C.: Summer 2009 wildfires in Portugal: emission of trace gases and aerosol composition, *Atmos. Environ.*, 45, 641–649, 2011.
- Andreae, M. O. and Merlet, P.: Emission of trace gases and aerosols from biomass burning, *Global Biogeochem. Cy.*, 15, 955–966, doi:10.1029/2000GB001382, 2001.
- Andreae, M. O., Artaxo, P., Brandão, C., Carswell, F. E., Caccioli, P., da Costa, A. L., Culf, A. D., Esteves, J. L., Gash, J. H. C., Grace, J., Kabat, P., Lelieveld, J., Malhi, Y., Manzi, A. O., Meixner, F. X., Nobre, A. D., Nobre, C., Ruivo, M. d. L. P., Silva-Dias, M. A., Stefani, P., Valentini, R., von Jouanne, J., and Waterloo, M. J.: Biogeochemical cycling

- of carbon, water, energy, trace gases and aerosols in Amazonia: The LBA-EUSTACH experiments, *J. Geophys. Res.*, 107, 8066, doi:10.1029/2001JD000524, 2002.
- 1865 Andreae, M. O. and Rosenfeld, D.: Aerosol–cloud–precipitation interactions. Part 1. The nature and sources of cloud-active aerosols, *Earth-Sci. Rev.*, 89, 13–41, 2008.
- Andreae, M. O., Artaxo, P., Beck, V., Bela, M., Gerbig, C., Longo, K., Munger, J. W., Wiedemann, K. T., and Wofsy, S. C.: Carbon monoxide and related trace gases and aerosols over the Amazon Basin during the wet and dry seasons, *Atmos. Chem. Phys.*, 12, 6041–6065, 2012.
- 1870 Andreae, M. O. and Ramanathan, V.: Climate’s dark forcings, *Science*, 340, 280–281, doi:10.1126/science.1235731, 2013.
- 1875 Artaxo, P., Rizzo, L. V., Brito, J. F., Barbosa, H. M. J., Arana, A., Sena, E. T., Cirino, G. G., Bastos, W., Martin, S. T., and Andreae, M. O.: Atmospheric aerosols in Amazonia and land use change: from natural biogenic to biomass burning conditions, *Faraday Discussions*, 165, 203–235, doi:10.1039/C3FD00052D, 2013.
- 1880 Aumont, B., Szopa, S., and Madronich, S.: Modelling the evolution of organic carbon during its gas-phase tropospheric oxidation: development of an explicit model based on a self generating approach, *Atmos. Chem. Phys.*, 5, 2497–2517, doi:10.5194/acp-5-2497-2005, 2005.
- Barriopedro, D., Fischer, E. M., Luterbacher, J., Trigo, R. M., and García-Herrera, R.: The hot summer of 2010: redrawing the temperature record map of Europe, *Science*, 332, 220–224, 2011.
- 1890 Bergström, R., Denier van der Gon, H. A. C., Prévôt, A. S. H., Yttri, K. E., and Simpson, D.: Modelling of organic aerosols over Europe (2002–2007) using a volatility basis set (VBS) framework: application of different assumptions regarding the formation of secondary organic aerosol, *Atmos. Chem. Phys.*, 12, 8499–8527, doi:10.5194/acp-12-8499-2012, 2012.
- 1895 Bertschi, I. T. and Jaffe, D. A.: Long-range transport of ozone, carbon monoxide, and aerosols in the NE Pacific troposphere during the summer of 2003: observations of smoke plumes from Asian boreal fires, *J. Geophys. Res.*, 110, D05303, doi:10.1029/2004JD005135, 2005.
- 1900 Bessagnet, B., Menut, L., Curci, G., Hodzic, A., Guillaume, B., Liousse, C., Moukhtar, S., Pun, B., Seigneur, C., and Schulz, M.: Regional modeling of carbonaceous aerosols over Europe – focus on secondary organic aerosols, *J. Atmos. Chem.*, 61, 175–202, 2009.
- 1905 Bond, T. C., Doherty, S. J., Fahey, D. W., Forster, P. M., Bernsten, T., DeAngelo, B. J., Flanner, M. G., Ghan, S., Kärcher, B., Koch, D., Kinne, S., Kondo, Y., Quinn, P. K., Sarofim, M. C., Schultz, M. G., Schulz, M., Venkataraman, C., Zhang, H., Zhang, S., Bellouin, N., Guttikunda, S. K., Hopke, P. K., Jacobson, M. Z., Kaiser, J. W., Klimont, Z., Lohmann, U., Schwarz, J. P., Shindell, D., Storelvmo, T., Warren, S. G., and Zender, C. S.: Bounding the role of black carbon in the climate system: a scientific assessment, *J. Geophys. Res.-Atmos.*, 118, 5380–5552, doi:10.1002/jgrd.50171, 2013.
- 1915 Bowman, F. M., Odum, J. R., Seinfeld, J. H., and Pandis, S. N.: Mathematical model for gas-particle partitioning of secondary organic aerosols, *Atmos. Environ.*, 31, 3921–3931, 1997.
- Cappa, C. D., and Wilson, K. R.: Evolution of organic aerosol mass spectra upon heating: Implications for OA phase and partitioning behavior, *Atmos. Chem. Phys.*, 11(5), 1895–1911, doi:10.5194/acp-11-1895-2011, 2011.
- Carter, W. P. L.: Development of the SAPRC-07 chemical mechanism, *Atmos. Environ.*, 44, 5324–5335, doi:10.1016/j.atmosenv.2010.01.026, 2010.
- Chacon-Madrid, H. J. and Donahue, N. M.: Fragmentation vs. functionalization: chemical aging and organic aerosol formation, *Atmos. Chem. Phys.*, 11, 10553–10563, doi:10.5194/acp-11-10553-2011, 2011.
- Chakrabarty, R. K., Moosmüller, H., Chen, L.-W. A., Lewis, K., Arnott, W. P., Mazzoleni, C., Dubey, M. K., Wold, C. E., Hao, W. M., and Kreidenweis, S. M.: Brown carbon in tar balls from smoldering biomass combustion, *Atmos. Chem. Phys.*, 10, 6363–6370, doi:10.5194/acp-10-6363-2010, 2010.
- Conard, S., Sukhinin, A., Stocks, B., Cahoon, D., Davidenko, E., and Ivanova, G.: Determining effects of area burned and fire severity on carbon cycling and emissions in Siberia, *Climatic Change*, 55, 197–211, 2002.
- Corrigan, A. L., Russell, L. M., Takahama, S., Äijälä, M., Ehn, M., Junninen, H., Rinne, J., Petäjä, T., Kulmala, M., Vogel, A. L., Hoffmann, T., Ebben, C. J., Geiger, F. M., Chhabra, P., Seinfeld, J. H., Worsnop, D. R., Song, W., Auld, J., and Williams, J.: Biogenic and biomass burning organic aerosol in a boreal forest at Hyytiälä, Finland, during HUMPPA-COPEC 2010, *Atmos. Chem. Phys.*, 13, 12233–12256, doi:10.5194/acp-13-12233-2013, 2013.
- Derognat, C., Beekmann, M., Baeumle, M., Martin, D., and Schmidt, H.: Effect of biogenic volatile organic compound emissions on tropospheric chemistry during the Atmospheric Pollution Over the Paris Area (ESQUIF) campaign in the Ile-de-France region, *J. Geophys. Res.-Atmos.*, 108, 8560, doi:10.1029/2001JD001421, 2003.
- Donahue, N. M., Robinson, A. L., Stanier, C. O., and Pandis, S. N.: Coupled partitioning, dilution, and chemical aging of semivolatile organics, *Environ. Sci. Technol.*, 40, 2635–2643, doi:10.1021/es052297c, 2006.
- Donahue, N. M., Kroll, J. H., Pandis, S. N., and Robinson, A. L.: A two-dimensional volatility basis set – Part 2: Diagnostics of organic-aerosol evolution, *Atmos. Chem. Phys.*, 12, 615–634, doi:10.5194/acp-12-615-2012, 2012.
- Dubovik, O., Lapyonok, T., Kaufman, Y. J., Chin, M., Ginoux, P., Kahn, R. A., and Sinyuk, A.: Retrieving global aerosol sources from satellites using inverse modeling, *Atmos. Chem. Phys.*, 8, 209–250, doi:10.5194/acp-8-209-2008, 2008.
- Elansky, N. F., Mokhov, I. I., Belikov, I. B., Berezina, E. V., Elokhov, A. S., Ivanov, V. A., Pankratova, N. V., Postlyakov, O. V., Safronov, A. N., Skorokhod, A. I., and Shumskii, R. A.: Gaseous admixtures in the atmosphere over Moscow during the 2010 summer, *Izv. Atmos. Ocean. Phys.*, 47, 672–681, doi:10.1134/S000143381106003X, 2011.
- EMEP/CEIP: Present state of emissions as used in EMEP models, available at: http://www.ceip.at/webdab_emepdatabase/emissions_emepmodels/ (last access: 25 March 2015), 2014.
- Engling, G., He, J., Betha, R., and Balasubramanian, R.: Assessing the regional impact of Indonesian biomass burning emissions based on organic molecular tracers and chemical mass balance modeling, *Atmos. Chem. Phys.*, 14, 8043–8054, doi:10.5194/acp-14-8043-2014, 2014.

- Enting, I. G.: Inverse Problems in Atmospheric Constituents Transport, Cambridge University Press, Cambridge, 2002.
- 1980 Farina, S. C., Adams, P. J., and Pandis, S. N.: Modeling global secondary organic aerosol formation and processing²⁰⁴⁰ with the volatility basis set: implications for anthropogenic secondary organic aerosol, *J. Geophys. Res.*, 115, D09202, doi:10.1029/2009JD013046, 2010.
- 1985 Fiebig, M., Stohl, A., Wendisch, M., Eckhardt, S., and Petzold, A.: Dependence of solar radiative forcing of forest fire aerosol on²⁰⁴⁵ ageing and state of mixture, *Atmos. Chem. Phys.*, 3, 881–891, doi:10.5194/acp-3-881-2003, 2003.
- 1990 Fokeeva, E. V., Safronov, A. N., Rakitin, V. S., Yurganov, L. N., Grechko, E. I., and Shumskii, R. A.: Investigation of the 2010 July–August fires impact on carbon monoxide atmospheric pol-²⁰⁵⁰lution in Moscow and its outskirts, estimating of emissions, *Izv. Atmos. Ocean. Phys.*, 47, 682–698, 2011.
- 1995 Folberth, G. A., Hauglustaine, D. A., Lathi re, J., and Brocheton, F.: Interactive chemistry in the Laboratoire de M t eorologie Dy-²⁰⁵⁵namique general circulation model: model description and im- pact analysis of biogenic hydrocarbons on tropospheric chem- istry, *Atmos. Chem. Phys.*, 6, 2273–2319, doi:10.5194/acp-6-2273-2006, 2006.
- 2000 Golitsyn, G. S., Gorchakov, G. I., Grechko, E. I., Semout-²⁰⁶⁰nikova, E. G., Rakitin, V. S., Fokeeva, E. V., Karpov, A. V., Kur- batov, G. A., Baikova, E. S., and Safrygina, T. P.: Extreme car- bon monoxide pollution of the atmospheric boundary layer in Moscow region in the summer of 2010, *Dokl. Earth Sci.*, 441, 1666–1672, 2012.
- 2005 Goodrick, S. L., Achtemeier, G. L., Larkin, N. K., Liu, Y., and²⁰⁶⁵ Strand, T. M.: Modelling smoke transport from wildland fires: a review, *Int. J. Wildland Fire*, 22, 83–94, doi:10.1071/WF11116, 2012.
- 2010 Grieshop, A. P., Logue, J. M., Donahue, N. M., and Robinson, A. L.:²⁰⁷⁰ Laboratory investigation of photochemical oxidation of organic aerosol from wood fires 1: measurement and simulation of organic aerosol evolution, *Atmos. Chem. Phys.*, 9, 1263–1277, doi:10.5194/acp-9-1263-2009, 2009a.
- 2015 Grieshop, A. P., Miracolo, M. A., Donahue, N. M., and Robin-²⁰⁷⁵son, A. L.: Constraining the volatility distribution and gas- particle partitioning of combustion aerosols using isothermal dilution and thermodynamic measurements, *Environ. Sci. Technol.*, 43, 4750–4756, doi:10.1021/es8032378, 2009b.
- 2020 Guenther, A., Karl, T., Harley, P., Wiedinmyer, C., Palmer, P. I.,²⁰⁸⁰ and Geron, C.: Estimates of global terrestrial isoprene emissions using MEGAN (Model of Emissions of Gases and Aerosols from Nature), *Atmos. Chem. Phys.*, 6, 3181–3210, doi:10.5194/acp-6-3181-2006, 2006.
- 2025 Heald, C. L., Jacob, D. J., Park, R. J., Russell, L. M., Huebert, B. J.,²⁰⁸⁵ Seinfeld, J. H., Liao, H., and Weber, R. J.: A large organic aerosol source in the free troposphere missing from current models, *Geophys. Res. Lett.*, 32, L18809, doi:10.1029/2005GL023831, 2005.
- 2030 Heil, A. and Goldammer, J. G.: Smoke-haze pollution: a review of the 1997 episode in South-east Asia, *Reg. Environ. Change*, 2, 24–37, doi:10.1007/s101130100021, 2001.²⁰⁹⁰
- Hennigan, C. J., Miracolo, M. A., Engelhart, G. J., May, A. A.,²⁰⁹⁵ Presto, A. A., Lee, T., Sullivan, A. P., McMeeking, G. R., Coe, H., Wold, C. E., Hao, W.-M., Gilman, J. B., Kuster, W. C., de Gouw, J., Schichtel, B. A., Collett Jr., J. L., Kreiden- weis, S. M., and Robinson, A. L.: Chemical and physical trans-²⁰⁹⁵ formations of organic aerosol from the photo-oxidation of open biomass burning emissions in an environmental chamber, *Atmos. Chem. Phys.*, 11, 7669–7686, doi:10.5194/acp-11-7669-2011, 2011.
- Hennigan, C. J., Westervelt, D. M., Riipinen, I., Engelhart, G. J.,²¹⁰⁰ Lee, T., Collett, J. L., Pandis, S. N., Adams, P. J., and Robin- son, A. L.: New particle formation and growth in biomass burn- ing plumes: an important source of cloud condensation nuclei, *Geophys. Res. Lett.*, 39, L09805, doi:10.1029/2012GL050930, 2012.
- Heringa, M. F., DeCarlo, P. F., Chirico, R., Tritscher, T., Dom-²¹⁰⁵men, J., Weingartner, E., Richter, R., Wehrle, G., Pr v t, A. S. H., and Baltensperger, U.: Investigations of primary and secondary particulate matter of different wood combustion appliances with a high-resolution time-of-flight aerosol mass spectrometer, *Atmos. Chem. Phys.*, 11, 5945–5957, doi:10.5194/acp-11-5945-2011, 2011.
- Hobbs, P. V., Sinha, P., Yokelson, R. J., Christian, T. J., Blake, D. R.,²¹¹⁰ Gao, S., Kirchstetter, T. W., Novakov, T., and Pilewskie, P.: Evolution of gases and particles from a savanna fire in South Africa, *J. Geophys. Res.*, 108, D13, doi:10.1029/2002JD002352, 2003.
- Hodzic, A., Madronich, S., Bohn, B., Massie, S., Menut, L., and²¹¹⁵ Wiedinmyer, C.: Wildfire particulate matter in Europe during summer 2003: meso-scale modeling of smoke emissions, trans- port and radiative effects, *Atmos. Chem. Phys.*, 7, 4043–4064, doi:10.5194/acp-7-4043-2007, 2007.
- Hodzic, A., Jimenez, J. L., Madronich, S., Aiken, A. C., Bessag-²¹²⁰net, B., Curci, G., Fast, J., Lamarque, J.-F., Onasch, T. B., Roux, G., Schauer, J. J., Stone, E. A., and Ulbrich, I. M.: Model- ing organic aerosols during MILAGRO: importance of biogenic secondary organic aerosols, *Atmos. Chem. Phys.*, 9, 6949–6981, doi:10.5194/acp-9-6949-2009, 2009.
- Hodzic, A., Jimenez, J. L., Madronich, S., Canagaratna, M. R., De-²¹²⁵Carlo, P. F., Kleinman, L., and Fast, J.: Modeling organic aerosols in a megacity: potential contribution of semi-volatile and inter- mediate volatility primary organic compounds to secondary organic aerosol formation, *Atmos. Chem. Phys.*, 10, 5491–5514, doi:10.5194/acp-10-5491-2010, 2010.
- Huffman, J. A., Docherty, K. S., Mohr, C., Cubison, M. J., Ul-²¹³⁰brich, I. M., Ziemann, P. J., Onasch, T. B., and Jimenez, J. L.: Chemically resolved volatility measurements of organic aerosol from different sources, *Environ. Sci. Technol.*, 43, 5351–5357, doi:10.1021/Es803539d, 2009.
- Huijnen, V., Flemming, J., Kaiser, J. W., Inness, A., Leit o, J.,²¹³⁵ Heil, A., Eskes, H. J., Schultz, M. G., Benedetti, A., Hadji- Lazaro, J., Dufour, G., and Eremenko, M.: Hindcast experi- ments of tropospheric composition during the summer 2010 fires over western Russia, *Atmos. Chem. Phys.*, 12, 4341–4364, doi:10.5194/acp-12-4341-2012, 2012.
- Huneeus, N., Chevallier, F., and Boucher, O.: Estimating aerosol²¹⁴⁰ emissions by assimilating observed aerosol optical depth in a global aerosol model, *Atmos. Chem. Phys.*, 12, 4585–4606, doi:10.5194/acp-12-4585-2012, 2012.
- Ichoku, C. and Kaufman, J. Y.: A method to derive smoke emission rates from MODIS fire radiative energy measurements, *IEEE T. Geosci. Remote*, 43, 2636–2649, 2005.
- IPCC: Summary for policymakers, in: *Climate Change 2013: The Physical Science Basis. Contribution of Working Group I to the*

- Fifth Assessment Report of the Intergovernmental Panel on Climate Change, edited by: Stocker, T. F., Qin, D., Plattner, G.,²¹⁵⁵ K., Tignor, M., Allen, S. K., Boschung, J., Nauels, A., Xia, Y., Bex, V., and Midgley, P. M., Cambridge University Press, Cambridge, UK, New York, NY, USA, 3–29, 2013.
- Jacobson, M. Z.: Strong radiative heating due to the mixing state of black carbon in atmospheric aerosols, *Nature*, 409, 695–697,²¹⁶⁰ doi:10.1038/35055518, 2001.
- Janjic, Z. I.: The step-mountain coordinate: physical package, *Mon. Weather Rev.*, 118, 1429–1443, 1990.
- Janjic, Z. I.: The step-mountain eta coordinate model: further developments of the convection, viscous sublayer and turbulence²¹⁶⁵ closure schemes, *Mon. Weather Rev.*, 122, 927–945, 1994.
- Jathar, S. H., Gordon, T. D., Hennigan, C. J., Pye, H. O. T., Poulriot, G., Adams, P. J., Donahue, N. M., and Robinson, A. L.: Unspeciated organic emissions from combustion sources and their influence on the secondary organic aerosol budget in the²¹⁷⁰ United States, *P. Natl. Acad. Sci. USA*, 111, 10473–10478, doi:10.1073/pnas.1323740111, 2014.
- Jimenez, J. L., Canagaratna, M. R., Donahue, N. M., Prevot, A. S. H., Zhang, Q., Kroll, J. H., DeCarlo, P. F., Allan, J. D., Coe, H., Ng, N. L., Aiken, A. C., Docherty, K. S., Ulbrich, I. M.,²¹⁷⁵ Grieshop, A. P., Robinson, A. L., Duplissy, J., Smith, J. D., Wilson, K. R., Lanz, V. A., Hueglin, C., Sun, Y. L., Tian, J., Laaksonen, A., Raatikainen, T., Rautiainen, J., Vaattovaara, P., Ehn, M., Kulmala, M., Tomlinson, J. M., Collins, D. R., Cubison, M. J., Dunlea, E. J., Huffman, J. A., Onasch, T. B., Alfarra, M. R.,²¹⁸⁰ Williams, P. I., Bower, K., Kondo, Y., Schneider, J., Drewnick, F., Borrmann, S., Weimer, S., Demerjian, K., Salcedo, D., Cottrell, L., Griffin, R., Takami, A., Miyoshi, T., Hatakeyama, S., Shimono, A., Sun, J. Y., Zhang, Y. M., Dzepina, K., Kimmel, J. R., Sueper, D., Jayne, J. T., Herndon, S. C., Trim²¹⁸⁵born, A. M., Williams, L. R., Wood, E. C., Middlebrook, A. M., Kolb, C. E., Baltensperger, U., and Worsnop, D. R.: Evolution of Organic Aerosols in the Atmosphere, *Science*, 326, 1525–1529, doi:10.1126/science.1180353, 2009.
- Jolleys, M. D., Coe, H., McFiggans, G., Taylor, J. W., O’Shea, S. J.,²¹⁹⁰ Le Breton, M., Bauguitte, S. J.-B., Moller, S., Di Carlo, P., Aruffo, E., Palmer, P. I., Lee, J. D., Percival, C. J., and Gallagher, M. W.: Properties and evolution of biomass burning organic aerosol from Canadian boreal forest fires, *Atmos. Chem. Phys.*, 15, 3077–3095, doi:10.5194/acp-15-3077-2015, 2015. ²¹⁹⁵
- Kaiser, J. W., Heil, A., Andreae, M. O., Benedetti, A., Chubarova, N., Jones, L., Morcrette, J.-J., Razinger, M., Schultz, M. G., Suttie, M., and van der Werf, G. R.: Biomass burning emissions estimated with a global fire assimilation system based on observed fire radiative power, *Biogeosciences*, 9,²²⁰⁰ 527–554, doi:10.5194/bg-9-527-2012, 2012.
- Keil, A. and Haywood, J. M.: Solar radiative forcing by biomass burning aerosol particles during SAFARI 2000: a case study based on measured aerosol and cloud properties, *J. Geophys. Res.*, 108, D13, doi:10.1029/2002JD002315, 2003. ²²⁰⁵
- Kiehl, J. T.: Twentieth century climate model response and climate sensitivity, *Geophys. Res. Lett.*, 34, L22710, doi:10.1029/2007GL031383, 2007. ²¹⁵⁰
- Kononov, I. B., Beekmann, M., Kuznetsova, I. N., Yurova, A., and Zvyagintsev, A. M.: Atmospheric impacts of the 2010 Russian²²¹⁰ wildfires: integrating modelling and measurements of an extreme air pollution episode in the Moscow region, *Atmos. Chem. Phys.*, 11, 10031–10056, doi:10.5194/acp-11-10031-2011, 2011.
- Kononov, I. B., Beekmann, M., D’Anna, B., and George, C.: Significant light induced ozone loss on biomass burning aerosol: evidence from chemistry-transport modeling based on new laboratory studies, *Geophys. Res. Lett.*, 39, L17807, doi:10.1029/2012GL052432, 2012.
- Kononov, I. B., Berezin, E. V., Ciais, P., Broquet, G., Beekmann, M., Hadji-Lazarou, J., Clerbaux, C., Andreae, M. O., Kaiser, J. W., and Schulze, E.-D.: Constraining CO₂ emissions from open biomass burning by satellite observations of co-emitted species: a method and its application to wildfires in Siberia, *Atmos. Chem. Phys.*, 14, 10383–10410, doi:10.5194/acp-14-10383-2014, 2014.
- Kononov, I. B., Berezin, E. V., Beekmann, M.: Effect of the photochemical self-interaction of carbonaceous aerosol originating from wildfires, *Izv. Atm. Ocean. Phy.*, accepted for publication, 2015.
- Kroll, M., Peters, W., Hooghiemstra, P., George, M., Clerbaux, C., Hurtmans, D., McInerney, D., Sedano, F., Bergamaschi, P., El Hajj, M., Kaiser, J. W., Fisher, D., Yershov, V., and Muller, J.-P.: How much CO was emitted by the 2010 fires around Moscow?, *Atmos. Chem. Phys.*, 13, 4737–4747, doi:10.5194/acp-13-4737-2013, 2013.
- Kroll, J. H., Ng, N. L., Murphy, S. M., Flagan, R. C., and Seinfeld, J. H.: Secondary organic aerosol formation from isoprene photooxidation, *Environ. Sci. Technol.*, 40, 1869–1877, doi:10.1021/es0524301, 2006.
- Kroll, J. H., Donahue, N. M., Jimenez, J. L., Kessler, S., Canagaratna, M. R., Wilson, K., Alteri, K. E., Mazzoleni, L. R., Wozniak, A. S., Bluhm, H., Mysak, E. R., Smith, J. D., Kolb, C. E., and Worsnop, D. R.: Carbon oxidation state as a metric for describing the chemistry of atmospheric organic aerosol, *Nature Chemistry*, 3, 133–139, doi:10.1038/nchem.948, 2011.
- Lane, T. E., Donahue, N. M., and Pandis, S. N.: Simulating secondary organic aerosol formation using the volatility basis-set approach in a chemical transport model, *Atmos. Environ.*, 42, 7439–7451, 2008.
- Langmann, B., Duncan, B., Textor, C., Trentmann, J., and van der Werf, G. R.: Vegetation fire emissions and their impact on air pollution and climate, *Atmos. Environ.*, 43, 107–116, doi:10.1016/j.atmosenv.2008.09.047, 2009.
- Lee-Taylor, J., Hodzic, A., Madronich, S., Aumont, B., Camredon, M., and Valorso, R.: Multiday production of condensing organic aerosol mass in urban and forest outflow, *Atmos. Chem. Phys.*, 15, 595–615, doi:10.5194/acp-15-595-2015, 2015.
- Leskinen, A., Portin, H., Komppula, M., Miettinen, P., Arola, A., Lihavainen, H., Hatakka, J., Laaksonen, A., and Lehtinen, K. E. J.: Overview of the research activities and results at Puijo semi-urban measurement station, *Boreal Environ. Res.*, 14, 576–590, 2009.
- Levy, R. C., Remer, L. A., Kleidman, R. G., Mattoo, S., Ichoku, C., Kahn, R., and Eck, T. F.: Global evaluation of the Collection 5 MODIS dark-target aerosol products over land, *Atmos. Chem. Phys.*, 10, 10399–10420, doi:10.5194/acp-10-10399-2010, 2010.
- Lipsky, E. M. and Robinson, A. L.: Effects of dilution on fine particle mass and partitioning of semivolatile organics in diesel exhaust and wood smoke, *Environ. Sci. Technol.*, 40, 155–162, doi:10.1021/Es050319p, 2006.

- Madronich, S., McKenzie, R. E., Bjorn, L. O., and Caldwell, M. M.: Changes in biologically active ultraviolet radiation reaching the earth's surface, *J. Photoch. Photobio. B*, 46, 5–19, 1998.
- Martin, S. T., Andreae, M. O., Artaxo, P., Baumgardner, D., Chen, Q., Goldstein, A. H., Guenther, A., Heald, C. L., Mayol-Bracero, O. L., McMurry, P. H., Pauliquevis, T., Pöschl, U., Prather, K. A., Roberts, G. C., Saleska, S. R., Dias, M. A. S., Spracklen, D., Swietlicki, E., and Trebs, I.: Sources and properties of Amazonian aerosol particles, *Rev. Geophys.*, 48, RG2002, doi:10.1029/2008RG000280, 2010.
- May, A. A., Levin, E. J. T., Hennigan, C. J., Riipinen, I., Lee, T., Collett Jr., J. L., Jimenez, J. L., Kreidenweis, S. M., and Robinson, A. L.: Gas-particle partitioning of primary organic aerosol emissions: 3. Biomass burning, *J. Geophys. Res.-Atmos.*, 118, 11327–11338, doi:10.1002/jgrd.50828, 2013.
- Mei, L., Xue, Y., de Leeuw, G., Guang, J., Wang, Y., Li, Y., Xu, H., Yang, L., Hou, T., He, X., Wu, C., Dong, J., and Chen, Z.: Integration of remote sensing data and surface observations to estimate the impact of the Russian wildfires over Europe and Asia during August 2010, *Biogeosciences*, 8, 3771–3791, doi:10.5194/bg-8-3771-2011, 2011.
- Menut, L., Bessagnet, B., Khvorostyanov, D., Beekmann, M., Blond, N., Colette, A., Coll, I., Curci, G., Foret, G., Hodzic, A., Mailler, S., Meleux, F., Monge, J.-L., Pison, I., Siour, G., Turquety, S., Valari, M., Vautard, R., and Vivanco, M. G.: CHIMERE 2013: a model for regional atmospheric composition modelling, *Geosci. Model Dev.*, 6, 981–1028, doi:10.5194/gmd-6-981-2013, 2013.
- Mielonen, T., Portin, H. J., Komppula, M., Leskinen, A., Tamminen, J., Ialongo, I., Hakkarainen, J., Lehtinen, K. E. J., and Arola, A.: Biomass burning aerosols observed in Eastern Finland during the Russian wildfires in summer 2010 – Part 2: Remote sensing, *Atmos. Environ.*, 45, 279–287, 2011.
- Murphy, B. N. and Pandis, S. N.: Simulating the formation of semivolatile primary and secondary organic aerosol in a regional chemical transport model, *Environ. Sci. Technol.*, 43, 4722–4728, doi:10.1021/es803168a, 2009.
- Murphy, B. N., Donahue, N. M., Fountoukis, C., Dall'Osto, M., O'Dowd, C., Kiendler-Scharr, A., and Pandis, S. N.: Functionalization and fragmentation during ambient organic aerosol aging: application of the 2-D volatility basis set to field studies, *Atmos. Chem. Phys.*, 12, 10797–10816, doi:10.5194/acp-12-10797-2012, 2012.
- Nenes, A., Pilinis, C., and Pandis, S.: ISORROPIA: a new thermodynamic model for inorganic multicomponent atmospheric aerosols, *Aquat. Geochem.*, 4, 123–152, 1998.
- Ortega, A. M., Day, D. A., Cubison, M. J., Brune, W. H., Bon, D., de Gouw, J. A., and Jimenez, J. L.: Secondary organic aerosol formation and primary organic aerosol oxidation from biomass-burning smoke in a flow reactor during FLAME-3, *Atmos. Chem. Phys.*, 13, 11551–11571, doi:10.5194/acp-13-11551-2013, 2013.
- Pankow, J.: An absorption model of the gas/aerosol partitioning involved in the formation of secondary organic aerosol, *Atmos. Environ.*, 28, 189–193, 1994.
- Péré, J. C., Bessagnet, B., Mallet, M., Waquet, F., Chiapello, I., Minvielle, F., Pont, V., and Menut, L.: Direct radiative effect of the Russian wildfires and its impact on air temperature and atmospheric dynamics during August 2010, *Atmos. Chem. Phys.*, 14, 1999–2013, doi:10.5194/acp-14-1999-2014, 2014.
- Petrenko, M., Kahn, R., Chin, M., Soja, A., Kucsera, T., and Harshvardhan: The use of satellite-measured aerosol optical depth to constrain biomass burning emissions source strength in the global model GOCART, *J. Geophys. Res.*, 117, D18212, doi:10.1029/2012JD017870, 2012.
- Popovicheva, O. B., Kireeva, E. D., Persiantseva, N. M., Timofeev, M. A., Kistler, M., Kopeikin, V. M., and Kasper-Giebl, A.: Physicochemical characterization of smoke aerosol during large-scale wildfires: extreme event of August 2010 in Moscow, *Atmos. Environ.*, 96, 405–414, doi:10.1016/j.atmosenv.2014.03.026, 2014.
- Portin, H. J., Mielonen, T., Leskinen, A., Arola, A., Pärjälä, E., Romakkaniemi, S., Laaksonen, A., Lehtinen, K. E. J., and Komppula, M.: Biomass burning aerosols observed in Eastern Finland during the Russian wildfires in summer 2010 – Part 1: In-situ aerosol characterization, *Atmos. Environ.*, 47, 269–278, doi:10.1016/j.atmosenv.2011.10.067, 2012.
- Pöschl, U., Rose, D., and Andreae, M. O.: Climatologies of cloud-related aerosols – Part 2: Particle hygroscopicity and cloud condensation nuclei activity, in: *Clouds in the Perturbed Climate System*, edited by: Heintzenberg, J. and Charlson, R. J., MIT Press, Cambridge, ISBN 978-0-262-01287-4, 58–72, 2009.
- Pun, B. K., Seigneur, C., and Lohmann, K.: Modeling secondary organic aerosol formation via multiphase partitioning with molecular data, *Environ. Sci. Technol.*, 40, 4722–4731, 2006.
- Remer, L. A., Kaufman, Y. J., Tanre, D., Mattoo, S., Chu, D. A., Martins, J. V., Li, R.-R., Ichoku, C., Levy, R. C., Kleidman, R. G., Eck, T. F., Vermote, E., and Holben, B. N.: The MODIS aerosol algorithm, products, and validation, *J. Atmos. Sci.*, 62, 947–973, 2005.
- Reid, J. S., Koppmann, R., Eck, T. F., and Eleuterio, D. P.: A review of biomass burning emissions part II: intensive physical properties of biomass burning particles, *Atmos. Chem. Phys.*, 5, 799–825, doi:10.5194/acp-5-799-2005, 2005a.
- Reid, J. S., Eck, T. F., Christopher, S. A., Koppmann, R., Dubovik, O., Eleuterio, D. P., Holben, B. N., Reid, E. A., and Zhang, J.: A review of biomass burning emissions part III: intensive physical properties of biomass burning particles, *Atmos. Chem. Phys.*, 5, 827–849, doi:10.5194/acp-5-827-2005, 2005b.
- Robinson, A. L., Donahue, N. M., Shrivastava, M. K., Weitkamp, E. A., Sage, A. M., Grieshop, A. P., Lane, T. E., Pierce, J. R., and Pandis, S. N.: Rethinking organic aerosols: semivolatile emissions and photochemical aging, *Science*, 315, 1259–1262, doi:10.1126/science.1133061, 2007.
- Saleh, R., Hennigan, C. J., McMeeking, G. R., Chuang, W. K., Robinson, E. S., Coe, H., Donahue, N. M., and Robinson, A. L.: Absorptivity of brown carbon in fresh and photo-chemically aged biomass-burning emissions, *Atmos. Chem. Phys.*, 13, 7683–7693, doi:10.5194/acp-13-7683-2013, 2013.
- Saleh, R., Robinson, E. S., Tkacik, D. S., Ahern, A. T., Liu, S., Aiken, A. C., Sullivan, R. C., Presto, A. A., Dubey, M. K., Yokelson, R. J., Donahue, N. M., and Robinson, A. L.: Brownness of organics in aerosols from biomass burning linked to their black carbon content, *Nat. Geosci.*, 7, 647–650, doi:10.1038/ngeo2220, 2014.
- Schutgens, N., Nakata, M., and Nakajima, T.: Estimating aerosol emissions by assimilating remote sensing observations into

- a global transport model, *Remote Sens.*, 4, 3528–3543, doi:10.3390/rs4113528, 2012.
- Seinfeld, J. H., and Pandis, S. N.: *Atmospheric Chemistry and Physics: from Air Pollution to Climate Change*, 2nd edn., Wiley-Interscience, J. Wiley & Sons, Inc., New York, 2006.
- Shiraiwa, M., Yee, L. D., Schilling, K. A., Loza, C. L., Craven, J. S., Zuend, A., Ziemann, P. J., and Seinfeld, J. H.: Size distribution dynamics reveal particle-phase chemistry in organic aerosol formation, *Proc. Natl. Acad. Sci. U.S.A.*, 110(29), 11,746–11,750, doi:10.1073/pnas.1307501110, 2013.
- Shrivastava, M. K., Lipsky, E. M., Stanier, C. O., and Robinson, A. L.: Modeling semivolatile organic aerosol mass emissions from combustion systems, *Environ. Sci. Technol.*, 40, 2671–2677, doi:10.1021/es0522231, 2006.
- Shrivastava, M., Fast, J., Easter, R., Gustafson Jr., W. I., Zaveri, R. A., Jimenez, J. L., Saide, P., and Hodzic, A.: Modeling organic aerosols in a megacity: comparison of simple and complex representations of the volatility basis set approach, *Atmos. Chem. Phys.*, 11, 6639–6662, doi:10.5194/acp-11-6639-2011, 2011.
- Shrivastava, M., Zelenyuk, A., Imre, D., Easter, R. C., Beranek, J., Zaveri, R. A., and Fast, J. D.: Implications of Low Volatility and Gas-phase Fragmentation Reactions on SOA Loadings and their Spatial and Temporal Evolution in the Atmosphere, *J. Geophys. Res. Atmos.*, 118(8), 3328–3342, doi:10.1002/jgrd.50160, 2013.
- Shrivastava, M., Easter, R., Liu, X., Zelenyuk, A., Singh, B., Zhang, K., Ma, P-L, Chand, D., Ghan, S., Jimenez, J. L., Zhang, Q., Fast, J., Rasch, P. and Tiitta, P.: Global transformation and fate of SOA: Implications of low volatility SOA and gas-phase fragmentation reactions, *J. Geophys. Res. Atmos.*, 120, 4169–4195, doi:10.1002/2014JD022563, 2015.
- Sinha, P., Hobbs, P. V., Yokelson, R. J., Blake, D. R., Gao, S., and Kirchstetter, T. W.: Distribution of trace gases and aerosols during the dry biomass burning season in southern Africa, *J. Geophys. Res.*, 108, D17, doi:10.1029/2003JD003691, 2003.
- Skamarock, W. C., Klemp, J. B., Dudhia, J., Gill, D. O., Barker, D. M., Wang, W., and Powers, J. G.: A description of the Advanced Research WRF Version 2, NCAR Tech Notes-468+STR, Boulder, Colorado, USA, 2005.
- Sofiev, M., Vankevich, R., Lotjonen, M., Prank, M., Petukhov, V., Ermakova, T., Koskinen, J., and Kukkonen, J.: An operational system for the assimilation of the satellite information on wildland fires for the needs of air quality modelling and forecasting, *Atmos. Chem. Phys.*, 9, 6833–6847, doi:10.5194/acp-9-6833-2009, 2009.
- Sofiev, M., Ermakova, T., and Vankevich, R.: Evaluation of the smoke-injection height from wild-land fires using remote-sensing data, *Atmos. Chem. Phys.*, 12, 1995–2006, doi:10.5194/acp-12-1995-2012, 2012.
- Strand, T. M., Larkin, N., Craig, K. J., Raffuse, S., Sullivan, D., Solomon, R., Rorig, M., Wheeler, N., and Pryden, D.: Analyses of BlueSky Gateway PM_{2.5} predictions during the 2007 southern and 2008 northern California fires, *J. Geophys. Res.*, 117, D17301, doi:10.1029/2012JD017627, 2012.
- Stevanovic, S., Miljevic, B., Surawski, N. C., Fairfull-Smith, K. E., Bottle, S. E., Brown, R., and Ristovski, Z. D.: Influence of Oxygenated Organic Aerosols (OOAs) on the oxidative potential of diesel and biodiesel particulate matter, *Environ. Sci. Technol.*, 47, 7655–7662, doi:10.1021/es4007433, 2013.
- Stohl, A., Williams, E., Wotawa, G., and Kromp-Kolb, H.: A European inventory of soil nitric oxide emissions and the effect of these emissions on the photochemical formation of ozone, *Atmos. Environ.*, 30, 3741–3755, doi:10.1016/1352-2310(96)00104-5, 1996.
- Tsimpidi, A. P., Karydis, V. A., Zavala, M., Lei, W., Molina, L., Ulbrich, I. M., Jimenez, J. L., and Pandis, S. N.: Evaluation of the volatility basis-set approach for the simulation of organic aerosol formation in the Mexico City metropolitan area, *Atmos. Chem. Phys.*, 10, 525–546, doi:10.5194/acp-10-525-2010, 2010.
- Vakkari, V., Kerminen, V.-M., Beukes, J. P., Tiitta, P., van Zyl, P. G., Josipovic, M., Venter, A. D., Jaars, K., Worsnop, D. R., Kulmala, M., and Laakso, L.: Rapid changes in biomass burning aerosols by atmospheric oxidation, *Geophys. Res. Lett.*, 41, 2644–2651, doi:10.1002/2014GL059396, 2014.
- van der Werf, G. R., Randerson, J. T., Giglio, L., Collatz, G. J., Mu, M., Kasibhatla, P. S., Morton, D. C., DeFries, R. S., Jin, Y., and van Leeuwen, T. T.: Global fire emissions and the contribution of deforestation, savanna, forest, agricultural, and peat fires (1997–2009), *Atmos. Chem. Phys.*, 10, 11707–11735, doi:10.5194/acp-10-11707-2010, 2010.
- van Donkelaar, A., Martin, R. V., Levy, R. C., da Silva, A. M., Krzyzanowski, M., Chubarova, N. E., Semutnikova, E., and Cohen, A. J.: Satellite-based estimates of ground-level fine particulate matter during extreme events: a case study of the Moscow fires in 2010, *Atmos. Environ.*, 45, 6225–6232, 2011.
- Vaden, T. D., Imre D., Beranek, J., Shrivastava, M., and Zelenyuk A.: Evaporation kinetics and phase of laboratory and ambient secondary organic aerosol, *Proc. Natl. Acad. Sci. U.S.A.*, 2190–2195, doi:10.1073/pnas.1013391108, 2011.
- Vautard, R., Bessagnet, B., Chin, M., and Menut, L.: On the contribution of natural aeolian sources to particulate matter concentrations in Europe: testing hypotheses with a modelling approach, *Atmos. Environ.*, 39, 3291–3303, 2005.
- Vicente, A., Alves, C., Calvo, A. I., Fernandes, A. P., Nunes, T., Monteiro, C., Almeida, S. M., and Pio, C.: Emission factors and detailed chemical composition of smoke particles from the 2010 wildfire season, *Atmos. Environ.*, 71, 295–303, doi:10.1016/j.atmosenv.2013.01.062, 2013.
- Wang, J., Christopher, S. A., Nair, U. S., Reid, J. S., Prins, E. M., Szykman, J., and Hand, J. L.: Mesoscale modeling of Central American smoke transport to the United States: 1. “Top-down” assessment of emission strength and diurnal variation impacts, *J. Geophys. Res.*, 111, D05S17, doi:10.1029/2005JD006416, 2006.
- Wiedinmyer, C., Quayle, B., Geron, C., Belote, A., McKenzie, D., Zhang, X. Y., O’Neill, S., and Wynne, K. K.: Estimating emissions from fires in North America for air quality modeling, *Atmos. Environ.*, 40, 3419–3432, 2006.
- Witte, J. C., Douglass, A. R., da Silva, A., Torres, O., Levy, R., and Duncan, B. N.: NASA A-Train and Terra observations of the 2010 Russian wildfires, *Atmos. Chem. Phys.*, 11, 9287–9301, doi:10.5194/acp-11-9287-2011, 2011.
- Wooster, M. J., Roberts, G., Perry, G. L. W., and Kaufman, Y. J.: Retrieval of biomass combustion rates and totals from fire radiative power observations: FRP derivation and calibration relationships between biomass consumption and fire radiative energy release, *J. Geophys. Res.*, 110, D24311, doi:10.1029/2005JD006318, 2005.

- Xu, X., Wang, J., Henze, D. K., Qu, W., and Kopacz, M.: Constraints on aerosol sources using GEOS-Chem adjoint and MODIS radiances, and evaluation with multisensor (OMI, MISR) data, *J. Geophys. Res.-Atmos.*, 118, 6396–6413, doi:10.1002/jgrd.50515, 2013.
- Yokelson, R. J., Crounse, J. D., DeCarlo, P. F., Karl, T., Urbanski, S., Atlas, E., Campos, T., Shinozuka, Y., Kapustin, V., Clarke, A. D., Weinheimer, A., Knapp, D. J., Montzka, D. D., Holloway, J., Weibring, P., Flocke, F., Zheng, W., Toohey, D., Wennberg, P. O., Wiedinmyer, C., Mauldin, L., Fried, A., Richter, D., Walega, J., Jimenez, J. L., Adachi, K., Buseck, P. R., Hall, S. R., and Shetter, R.: Emissions from biomass burning in the Yucatan, *Atmos. Chem. Phys.*, 9, 5785–5812, doi:10.5194/acp-9-5785-2009, 2009.
- Zhang, Q. J., Beekmann, M., Drewnick, F., Freutel, F., Schneider, J., Crippa, M., Prevot, A. S. H., Baltensperger, U., Poulain, L., Wiedensohler, A., Sciare, J., Gros, V., Borbon, A., Colomb, A., Michoud, V., Doussin, J.-F., Denier van der Gon, H. A. C., Haffelin, M., Dupont, J.-C., Siour, G., Petetin, H., Bessagnet, B., Pandis, S. N., Hodzic, A., Sanchez, O., Honoré, C., and Perrussel, O.: Formation of organic aerosol in the Paris region during the MEGAPOLI summer campaign: evaluation of the volatility-basis-set approach within the CHIMERE model, *Atmos. Chem. Phys.*, 13, 5767–5790, doi:10.5194/acp-13-5767-2013, 2013.
- Zhang, S., Penner, J. E., and Torres, O.: Inverse modeling of biomass burning emissions using Total Ozone Mapping Spectrometer aerosol index for 1997, *J. Geophys. Res.*, 110, D21306, doi:10.1029/2004JD005738, 2005.
- Zhang, Y., Huang, J.-P., Henze, D. K., and Seinfeld, J. H.: Role of isoprene in secondary organic aerosol formation on a regional scale, *J. Geophys. Res.-Atmos.*, 112, D20207, doi:10.1029/2007JD008675, 2007.

Table 1. Two types of volatility distributions (f_i) used in this study for specifying emissions of POA species from fires. The distributions are based on the data by May et al. (2013) and were used together with the recommended values of the accommodation coefficient and the enthalpies ($\gamma = 1.0$, $H_{vap} = 85 - 4 \log C_i^*$).

C_i^*	Volatility distribution type	
	A	B
10^{-2}	0.2	0.1
10^{-1}	0.0	0.0
1	0.1	0.05
10	0.1	0.05
10^2	0.2	0.2
10^3	0.1	0.15
10^4	0.3	0.45

Table 2. Biomass burning emission factors (β , g kg^{-1}) specified in the emission model (see Eq. 3) for different types of vegetative land cover. The data are based on Andreae and Merlet (2001) and subsequent updates.

	agricultural burning	grassland	forest
OC	4.2	3.1	7.7
BC	0.42	0.55	0.58
CO	95	65	115
NMHC	9.9	5.5	8.7
NO _x	2.44	2.49	3.10

Table 3. Simulation settings for the different modelling scenarios with emissions from fires. The corresponding two types (A and B) of volatility distributions are specified in Table 1. Note that along with the simulations based on the “fire” scenarios listed in the table, an additional model run (“BGR”) was made to simulate “background” conditions in the absence of fire emissions (see Sect. 2.8). SVOC: semi-volatile organic compounds; VOC: volatile organic compounds; POA: primary organic aerosol species, S-SOA: SVOC produced from oxidation of POA; V-SOA: SVOC produced from oxidation of VOC.

Modeling scenario	Specifications
STN	no oxidation of SVOC; POA species are non-volatile and chemically inert
VBS-1	multi-generation gas-phase SVOC oxidation scheme based on Grieshop et al. (2009b) (a two-bin shift in volatility and a 40 % mass increase as a result of each reaction of POA(g) or S-SOA(g) with OH, $k_{\text{OH}} = 2 \times 10^{-11} \text{ cm}^3 \text{ s}^{-1}$); the type A volatility distribution (May et al., 2013), multi-stage oxidation of “traditional” VOC precursors of V-SOA (Zhang et al., 2013)
VBS-2	the same as VBS-1, but with the type B volatility distribution (a larger fraction of more volatile POA is assumed)
VBS-3	the same as VBS-2, but with the fragmentation and condensed-phase transformation processes taken into account following Shrivastava et al. (2013) (with some modifications explained in Sect. 2.4.3)
VBS-4	the same as VBS-2, but with a single-generation oxidation scheme described in Jathar et al. (2014) (POA is chemically represented by a surrogate species, such as n-pentadecane, that also represents 10 % of the total VOC (non-methane) emissions from biomass burning)
VBS-5	the same as VBS-1, but without any oxidation of SVOC

Table 4. Characteristics of the simulation data (after bias correction) compared to air pollution measurements at monitoring stations in the Moscow region. F_α are the optimal estimates for the fire emission correction factor (see Eq. 4) derived from PM_{10} data; the geometric SD characterizing uncertainties in F_α are given in parentheses. $\overline{\text{PM}}_{10}$ is the mean PM_{10} concentration over the study period. $[\Delta\text{PM}_{10}/\Delta\text{CO}]_{\text{fit}}$ is the normalized excess mixing ratio evaluated as the slope of a linear fit to the relationship between perturbations of CO and PM_{10} concentrations due to fire emissions on days affected by fires (see also Fig. 7).

Characteristic	Observations	Simulation scenario					
		STN	VBS-1	VBS-2	VBS-3	VBS-4	VBS-5
F_α	N/A	1.03(1.09)	1.03(1.06)	1.05(1.09)	1.18(1.10)	1.27(1.16)	1.54(1.11)
$\overline{\text{PM}}_{10}$ [$\mu\text{g m}^{-3}$]	123	102	104	106	104	101	100
RMSE [$\mu\text{g m}^{-3}$]	N/A	81.5	80.1	78.9	80.4	84.1	84.0
r	N/A	0.86	0.86	0.86	0.86	0.85	0.85
$[\Delta\text{PM}_{10}/\Delta\text{CO}]_{\text{fit}}$, [g g^{-1}]	0.069	0.068	0.067	0.067	0.068	0.067	0.067

Table 5. Characteristics of simulation data (after bias correction) compared to air pollution measurements at the Maaherrankatu site in Kuopio.

Characteristic	Observations	Simulation scenario					
		STN	VBS-1	VBS-2	VBS-3	VBS-4	VBS-5
$\overline{\text{PM}}_{10}$ [$\mu\text{g m}^{-3}$]	17.5	15.8	17.4	18.1	17.3	16.1	15.5
RMSE [$\mu\text{g m}^{-3}$]	N/A	7.25	6.26	6.74	6.31	7.44	7.65
r	N/A	0.91	0.89	0.88	0.89	0.87	0.91
$[\Delta\text{PM}_{10}/\Delta\text{CO}]_{\text{fit}}$, [g g^{-1}]	0.18	0.09	0.11	0.15	0.13	0.10	0.07

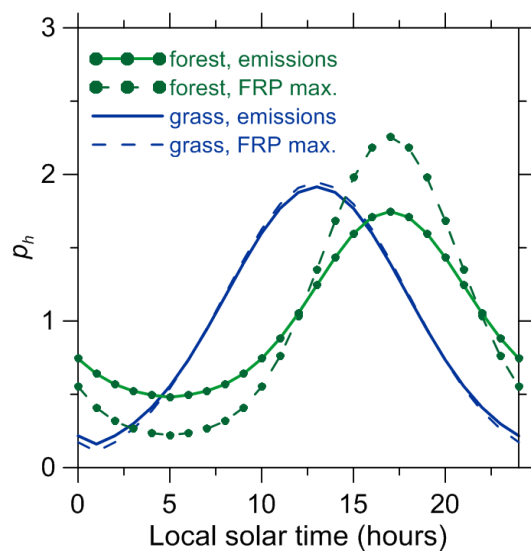


Figure 1. Diurnal profiles of fire emissions ($h_e(t)$) and daily FRP maxima ($h_m(t)$) used in the emission model (see Eqs. 3 and 5).

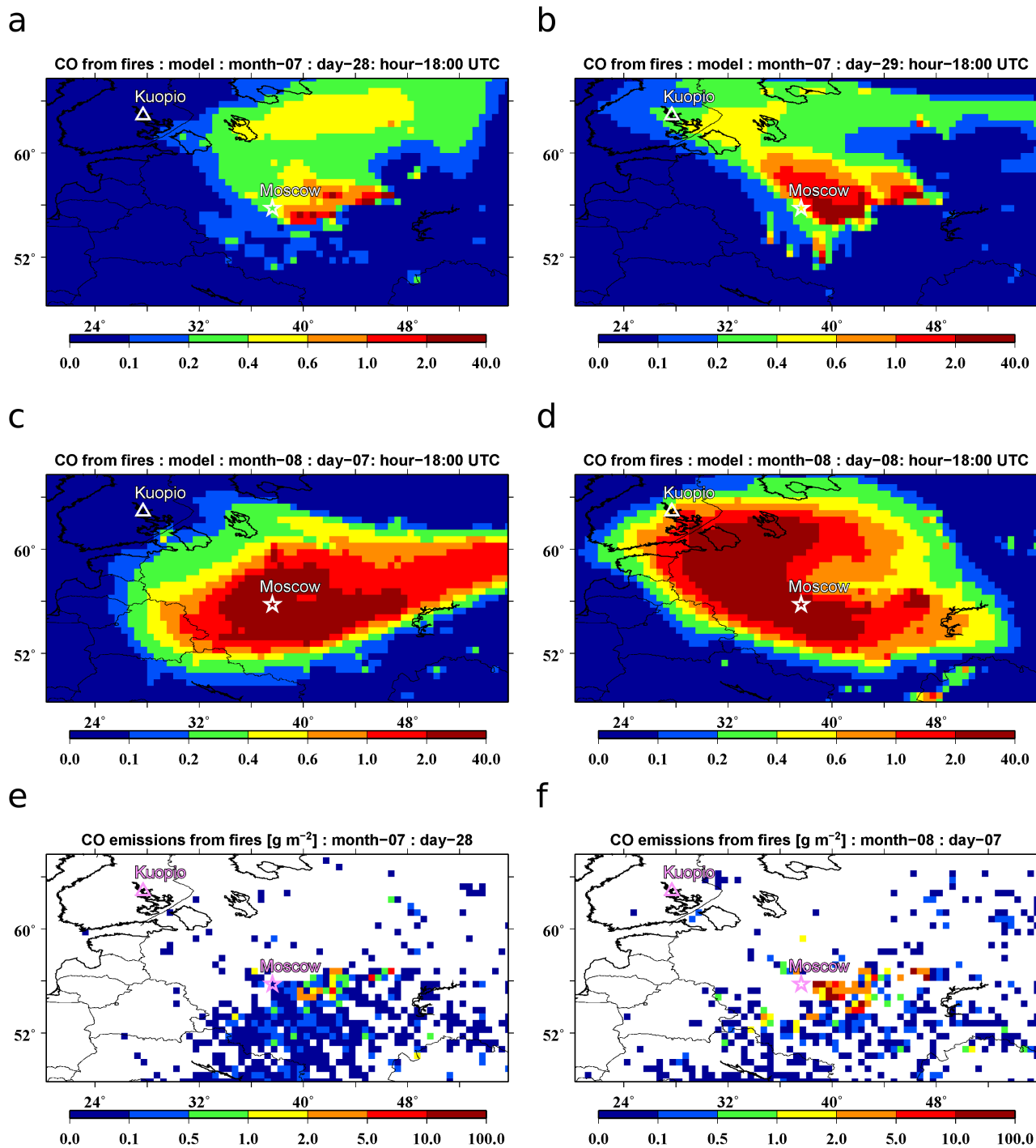


Figure 2. Simulated near-surface concentration (mg m^{-3}) of fire-emitted CO at 18:00 UTC on (a, b) 28 and 29 July and on (c, d) 7 and 8 August 2010, respectively, along with spatial distributions of CO amounts (g m^{-2}) emitted from fires on (e) 28 July and (f) 7 August 2010.

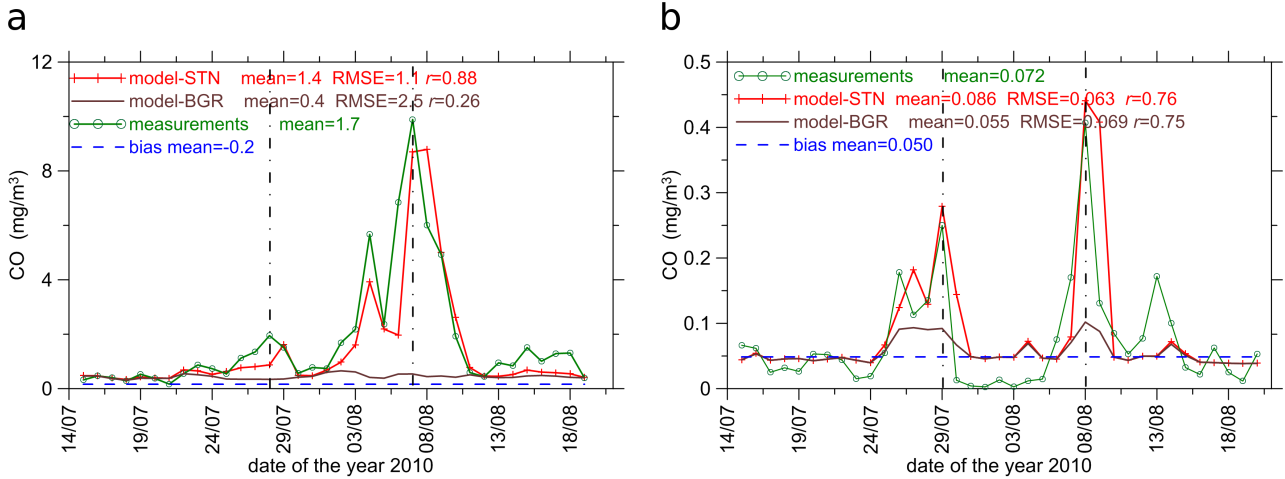


Figure 3. Time series of daily CO concentrations in Moscow (a) and in Kuopio (b). The CO concentration for the simulation scenario “STN” (see the red lines with crosses) are obtained by taking into account both anthropogenic and fire emissions (as explained in Sect. 2.8), while that for the “BGR” run (see the solid brown lines) reflects only anthropogenic CO emissions (along with other sources contributing to the boundary conditions for CO). The dashed blue lines depict the model bias (representing the systematic difference between the simulations and measurements on days not affected by fires); note that a negative bias (specifically, in the plot “a”) is shown with the opposite sign. The measurement data (from Mosecomonitoring stations and the Maaherrankatu site in Kuopio) are shown by green lines. The vertical dashed lines indicate the CO concentrations observed (a) in Moscow on 28 July and 7 August and (b) in Kuopio on 29 July and 8 August.

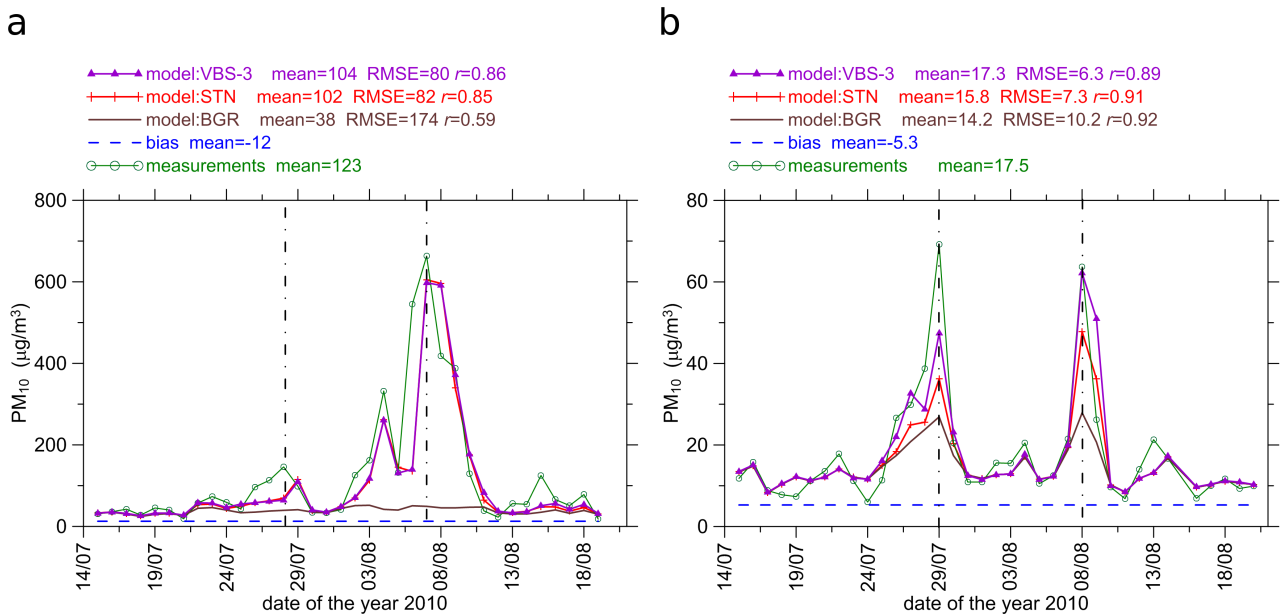


Figure 4. The same as in Fig. 3 but for PM₁₀ concentrations, except that in addition to results for the STN and BGR runs, this figure also shows (by a purple line) results for the VBS-3 run.

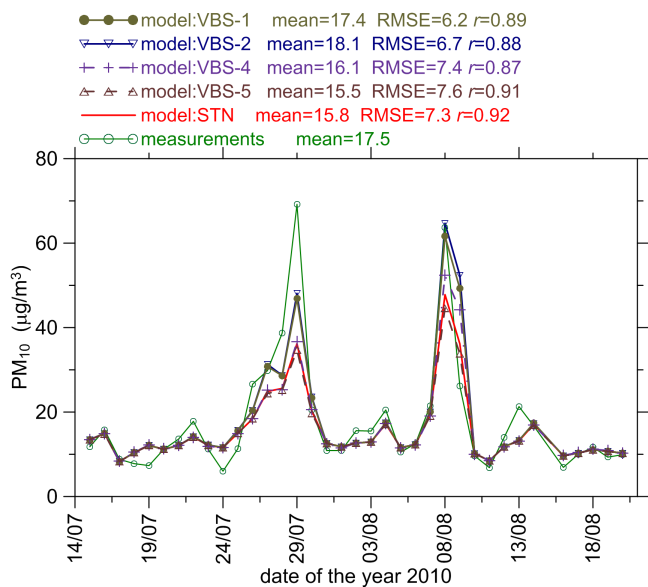


Figure 5. Time series of daily PM_{10} concentrations according to different simulation scenarios in comparison with measurements in Kuopio. Note that the time series for the VBS-3 scenario, which is shown in Fig. 4b, is omitted in this figure. Note also that the fire emissions for each scenario were fitted independently to measurements in the Moscow region (see the estimates of the emission correction factor, F_{α} , in Table 4 and the respective remark in Sect. 2.8).

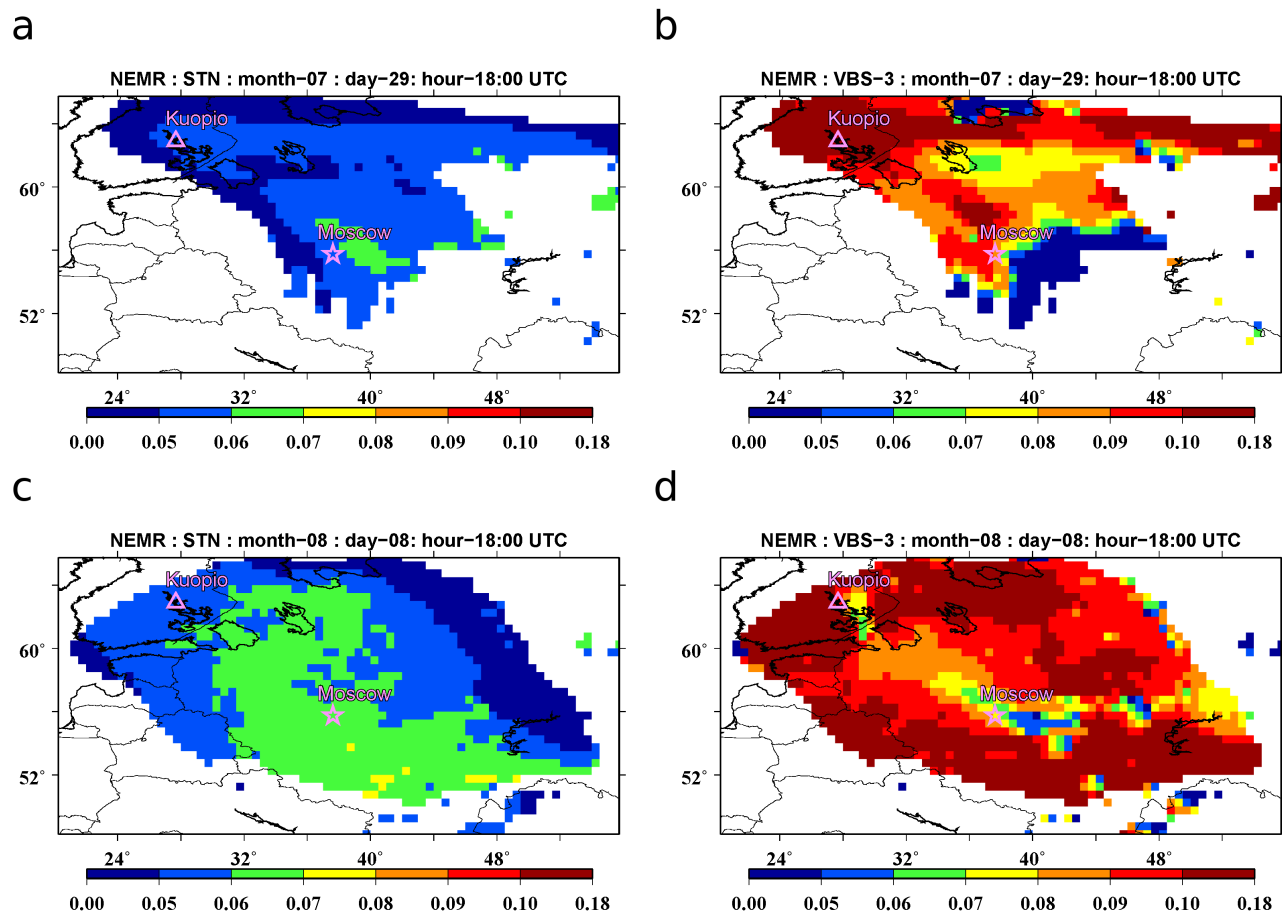


Figure 6. Normalized excess mixing ratio (NEMR) calculated as the ratio of near-surface mass concentrations of PM₁₀ and CO (g g^{-1}) originating from the fires. The NEMR values are shown only in the grid cells with CO concentrations exceeding $100 \mu\text{g m}^{-3}$ for 29 July (a, b) and 8 August (c, d) 2010 according to the STN (a, c) and VBS-3 (b, d) scenarios.

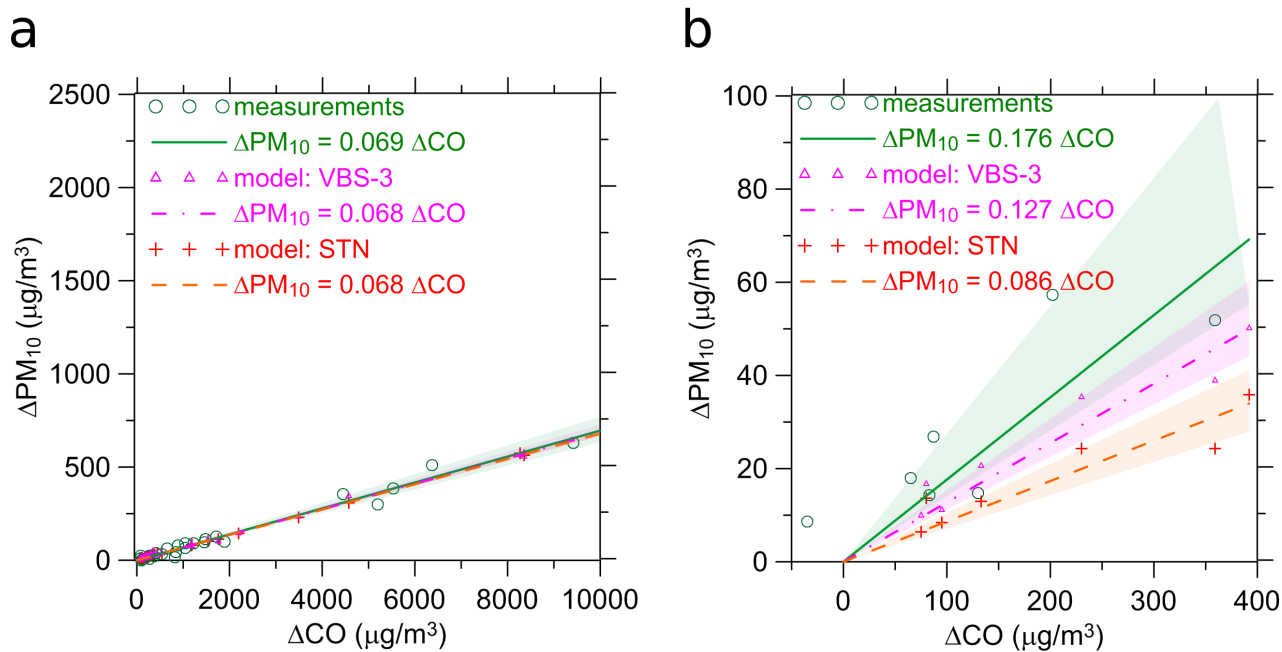


Figure 7. Scatter plots of the enhancements of PM₁₀ and CO concentrations (ΔPM_{10} and ΔCO) in (a) Moscow and (b) Kuopio on days affected by smoke from fires. Note that the relative scales of the ΔPM_{10} and ΔCO values are the same in both plots. The slope of a linear fit (through the origin) to the data provides an estimate of NEMR (see Sect. 3.1). The shaded areas depict uncertainties of the fits at the 95 % confidence level.

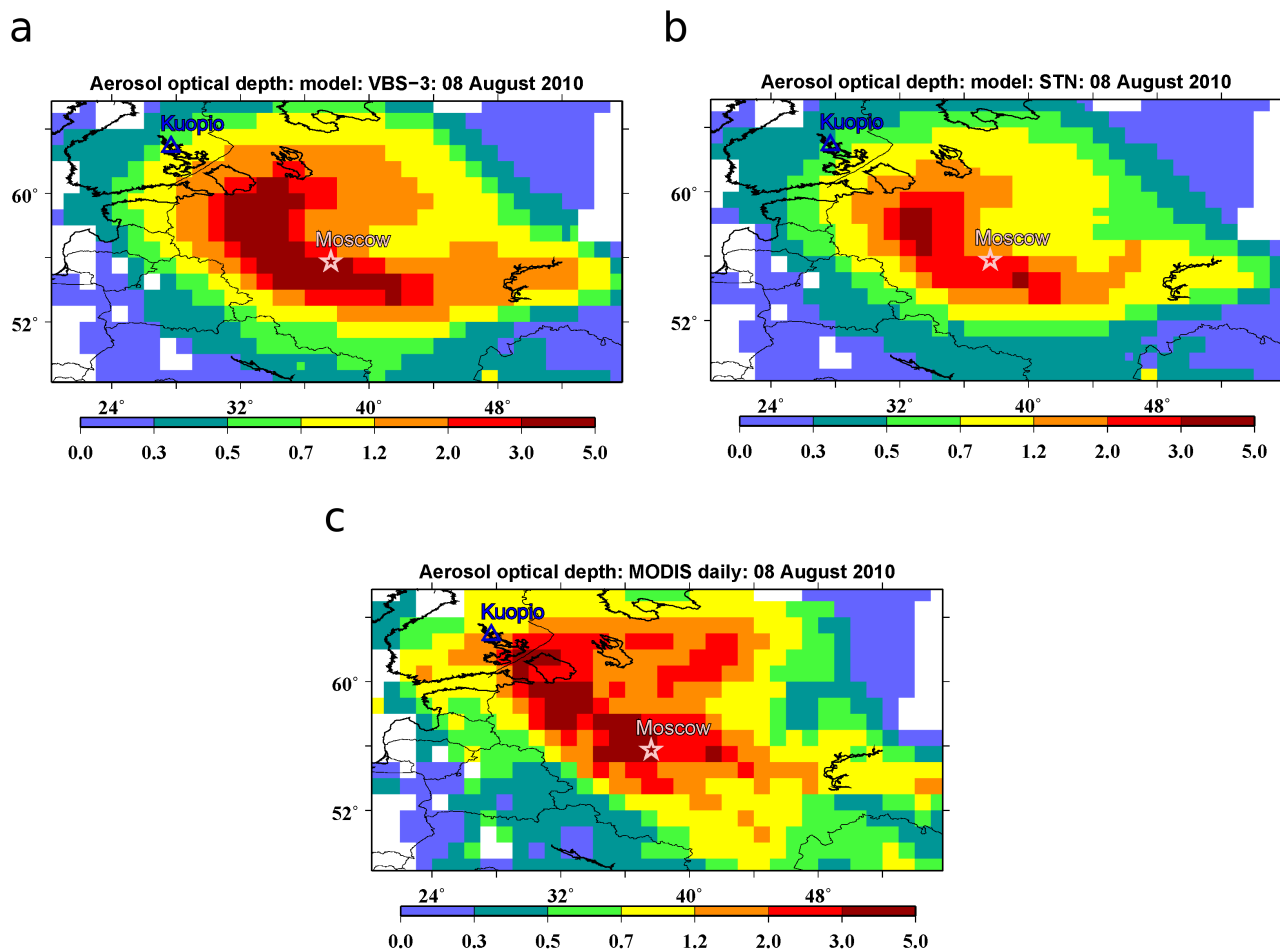


Figure 8. Spatial distributions of AOD at 550 nm on 8 August 2010 according to simulations for the scenarios “VBS-3” (a) and “STN” (b) in comparison with the MODIS measurement data (c).

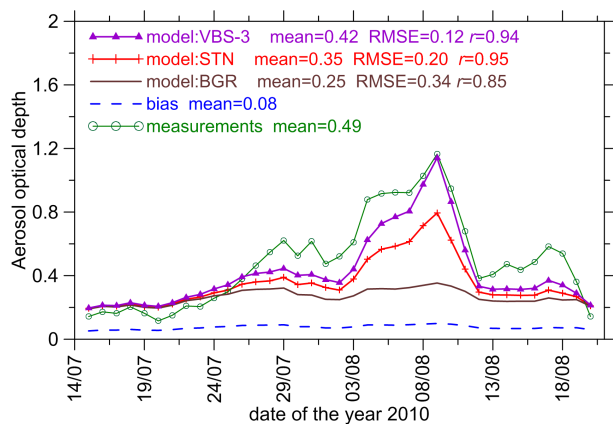


Figure 9. Time series of AOD at 550 nm obtained from simulations made with different scenarios and derived from the MODIS measurements. The daily data are averaged over the whole study region (see Fig. 8).

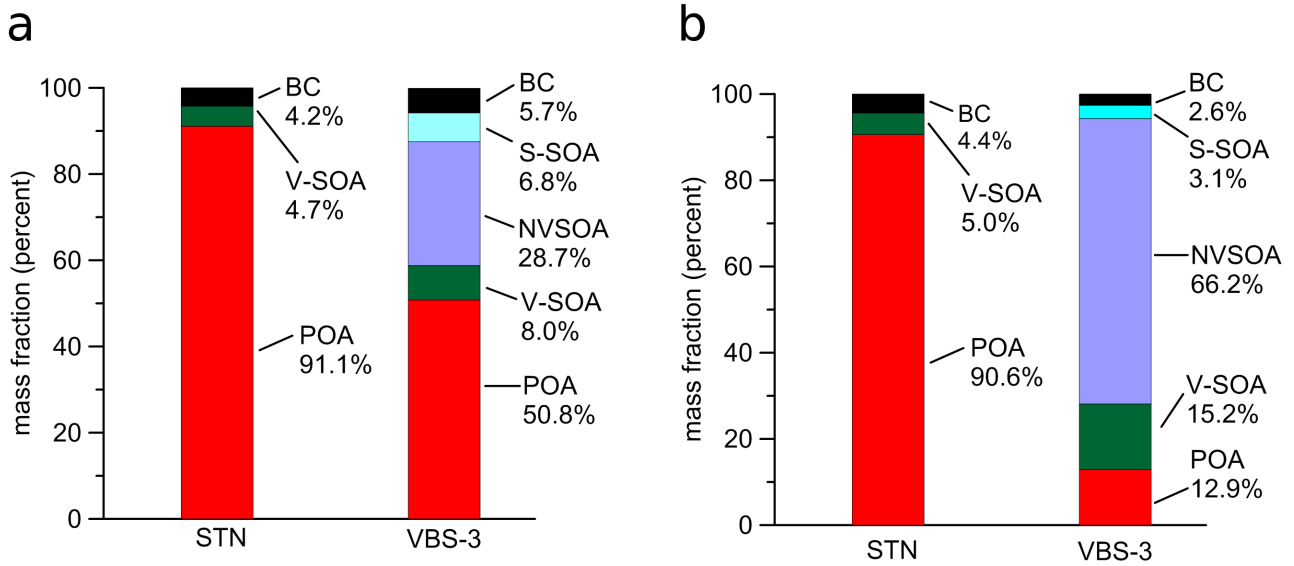


Figure 10. Composition of BB aerosol including primary organic aerosol (POA) species, secondary organic aerosol (SOA) species formed from oxidation of POA (S-SOA), secondary organic aerosol species formed from volatile organic compounds (V-SOA), non-volatile SOA species (NVSOA) assumed to be formed from the condensed-phase transformation of S-SOA species, and black carbon (BC), according to the simulation scenarios “STN” and “VBS-3” (a) in Moscow (at 18:00 UTC on 7 August 2010) and (b) in Kuopio (at 18:00 UTC on 8 August 2010).

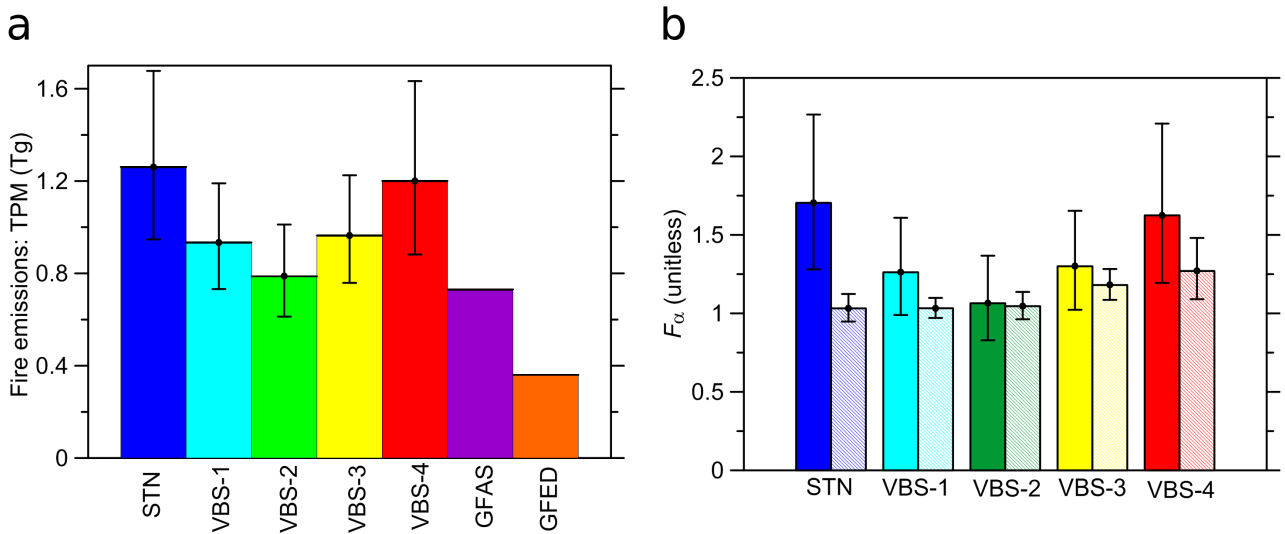


Figure 11. (a) Top-down estimates (in Tg) of total BB aerosol emissions from the study region in the period from 1 July to 31 August 2010 according to different simulation scenarios and in comparison with total particulate matter (TPM) emission data from the GFASv1.0 and GFED3.1 inventories. The estimates are derived from the MODIS AOD measurements. (b) The corresponding optimal estimates of F_α derived from MODIS (boxes with solid filling) measurements in comparison with corresponding estimates (boxes with dashed filling) obtained from ground-based measurements in the Moscow region. Note that the estimates for the “unrealistic” scenario “VBS-5”, which would exceed the axis limits (see Sect. 3.4), are not shown.